Available online at www.sciencedirect.com
ScienceDirect
Planetary and Space Science 58 (2010) 201–223
Planetary and Space Science
www.elsevier.com/locate/pss

PHEBUS: A double ultraviolet spectrometer to observe Mercury's exosphere

E. Chassefière[a,*], J.-L. Maria[a], J.-P. Goutail[a], E. Quémerais[a,b], F. Leblanc[a], S. Okano[c], I. Yoshikawa[d], O. Korablev[e], V. Gnedykh[e], G. Naletto[f], P. Nicolosi[f], M.-G. Pelizzo[f], J.-J. Correia[a], S. Gallet[a], C. Hourtoule[a], P.-O. Mine[a], C. Montaron[a], N. Rouanet[a], J.-B. Rigal[a], G. Muramaki[d], K. Yoshioka[d], O. Kozlov[e], V. Kottsov[e], P. Moisseev[g], N. Semena[e], J.-L. Bertaux[a], M.-Th. Capria[h], J. Clarke[i], G. Cremonese[j], D. Delcourt[k], A. Doressoundiram[l], S. Erard[l], R. Gladstone[m], M. Grande[n], D. Hunten[o], W. Ip[p], V. Izmodenov[q,e], A. Jambon[r], R. Johnson[s], E. Kallio[t], R. Killen[u], R. Lallement[a], J. Luhmann[v], M. Mendillo[i], A. Milillo[w], H. Palme[x], A. Potter[y], S. Sasaki[d], D. Slater[m], A. Sprague[o], A. Stern[m], N. Yan[a]

[a] *Service d'Aéronomie/IPSL, UPMC Univ. Paris 06, CNRS, UVSQ, Paris, France*
[b] *Institut d'Astrophysique Spatiale, Université Paris Sud, Orsay, France*
[c] *Tohoku University, Japan*
[d] *University of Tokyo, Japan*
[e] *Space Research Institute (IKI), Moscow, Russia*
[f] *LUXOR-CNR-INFM DEI University of Padova, Italy*
[g] *Astron Electronics, Orel, Russia*
[h] *INAF—IASF, Roma, Italy*
[i] *Department of Astronomy and Center for Space Physics, Boston University, USA*
[j] *INAF—Osservatorio Astronomico Padova, Italy*
[k] *CETP, Saint Maur des Fossés, France*
[l] *LESIA, Observatoire de Paris, France*
[m] *Southwest Research Institute, San Antonio, USA*
[n] *Rutherford Appleton Laboratory, UK*
[o] *Lunar and Planetary Laboratory, University of Arizona, Tucson, USA*
[p] *Institute of Astronomy, National Central University, Chung-Li, Taiwan*
[q] *Moscow State University, Moscow, Russia*
[r] *MAGIE, UPMC Univ. Paris 06, Paris, France*
[s] *Engineering Physics, University of Virginia, USA*
[t] *Finnish Meteorological Institute, Space Research Unit, Finland*
[u] *Department of Astronomy, University of Maryland, College Park, USA*
[v] *Space Sciences Laboratory, University of California, USA*

Abbreviations: AFM, atomic force microscopy; CVD, chemical vapor deposition; DPU, data processing unit; EO mode, exospheric along-orbit mode; ES mode, exospheric scanning mode; ET mode, exospheric twilight mode; EUV, extreme ultra-violet; FPGA, field-programmable gate array; FUV, far ultra-violet; HK, housekeeping; HK-IF, housekeeping interface; HT-MLI, high-temperature multi-layer insulation; IFOV, instrument field of view; IUE, International ultraviolet explorer; LAMP, Lyman alpha mapping project (on lunar reconnaissance orbiter); LOS, line-of-sight; MCP, micro-channel plate; MIXS, Mercury imaging X-ray spectrometer; MLI, multi-layer insulation; MMO, Mercury Magnetospheric Orbiter; MPO, Mercury Planetary Orbiter; MPPE, Mercury Plasma Particle Experiment; MSASI, Mercury Sodium Atmospheric Spectral Imager; NUV, near ultra-violet; OMEGA, Observatoire. pour la Minéralogie, l'Eau, les Glaces et l'Activité (on Mars-Express); PHEBUS, probing of Hermean exosphere by ultraviolet spectroscopy; PICAM, planetary ion camera; PM, photo-multiplier; RAE, resistive anode encoder; RGA, residual gas analysis; SERENA, Search for exosphere refilling and emitted neutral abundances; SL mode, surface Lyman-alpha mode; TIS, total integrated scatter; TM/TC, telemetry/telecommand.

*Corresponding author at: Service d'Aéronomie, Université Paris 6, Aile 45-46, 4ème étage, boîte 102, 4 place Jussieu 75252 Paris Cedex 05, France. Tel.: +33 1 44 27 37 53; fax: +33 1 44 27 37 76.
E-mail address: eric.chassefiere@aero.jussieu.fr (E. Chassefière).

0032-0633/$ - see front matter
doi:10.1016/j.pss.2008.05.018

[w]INAF—IFSI, Roma, Italy
[x]Universität zu Köln, Institut für Mineralogie und Geochemie, Köln, Germany
[y]National Solar Observatory, Tucson, USA

Received 4 February 2008; received in revised form 19 May 2008; accepted 23 May 2008
Available online 11 June 2008

Abstract

Probing of Hermean exosphere by ultraviolet spectroscopy (PHEBUS) is a double spectrometer for the Extreme Ultraviolet range (55–155 nm) and the Far Ultraviolet range (145–315 nm) devoted to the characterization of Mercury's exosphere composition and dynamics, and surface–exosphere connections. This French-led instrument is implemented in a cooperative scheme involving Japan (detectors), Russia (scanner) and Italy (ground calibration). PHEBUS will address the following main scientific objectives relative to Mercury's exosphere: determination of the composition and the vertical structure of the exosphere; characterization of the exospheric dynamics: day to night circulation, transport between active and inactive regions; study of surface release processes; identification and characterization of the sources of exospheric constituents; detection and characterization of ionized species and their relation with the neutral atmosphere; space and time monitoring of exosphere/magnetosphere exchange and transport processes; study and quantification of escape, global scale source/sink balance and geochemical cycles synergistically with other experiments of BepiColombo (Mercury Sodium Atmospheric Spectral Imager (MSASI), Mercury Plasma Particle Experiment (MPPE) on Mercury Magnetospheric Orbiter (MMO); Mercury imaging X-ray spectrometer (MIXS), Search for exosphere refilling and emitted neutral abundance (SERENA) on Mercury Planetary Orbiter (MPO)). Two gratings and two detectors are used according to a specific, compact design. The spectrum detection is based on the photon counting method and is realized using micro-channel plate (MCP) detectors with Resistive Anode Encoder (RAE). Typical photocathodes are CsI or KBr for the extreme ultra-violet (EUV) range, CsTe for the far ultra-violet (FUV) range. Extra visible lines are monitored using a photo-multiplier (PM) that is also used in photon counting mode. In order to prevent sensitivity losses which are critical in UV ranges, a minimum of reflections is achieved inside the instrument using only an off-axis parabola and a set of holographic gratings. A one degree-of-freedom scanning system allows to probe, at the highest possible signal-to-noise ratio, selected regions and altitude ranges of interest. Different modes of observation will be used sequentially (vertical scans, along-orbit scans, grazing observations at twilight, etc.). During the mission, the instrument will be regularly calibrated on well chosen stars, in such a way to quantitatively estimate the overall degradation of the sensitivity of the instrument.

Keywords: Mercury; Exosphere; Ultraviolet; Spectroscopy; BepiColombo

1. Introduction

Mercury's exosphere has been observed for the first time by Mariner 10 during its three flybys. Only three species were clearly identified, two of which, the hydrogen and helium atomic species, being most probably of solar wind origins (Broadfoot et al., 1974). The third one, oxygen atomic species, was observed at the limit of detection of the instrument (Broadfoot et al., 1976). Three other species have been later observed from Earth ground-based telescope, atomic sodium (Potter and Morgan, 1985), potassium (Potter and Morgan, 1987) and calcium (Bida et al., 2000). All together these species represent a maximum of few 10^5 atoms per cm^3 (Leblanc et al., 2007) which makes Mercury's exosphere a good analogy of the Moon surface bounded exosphere (Stern, 1999). All these species have been observed through resonant emission, the hydrogen, helium and oxygen in the UV, the calcium in the visible and near UV and the sodium and potassium in visible light. Mariner 10 also provided few clues on the thermal structure of Mercury's exosphere showing in particular an altitude profile of the hydrogen exosphere composed of a thermal (which may be due to surface reflected light) component and of a component hotter than the surface. Few sodium ground-based observations have also suggested that Mercury's sodium exosphere might be more energetic than if it was thermally accommodated with the surface (Killen et al., 1999).

Obviously, by the time this paper will be published, a fourth flyby by a spacecraft, MESSENGER, will have occurred with on board much better adapted instruments to detect and characterize Mercury's exosphere (in particular a UV spectrometer), so that hopefully our poor present understanding of Mercury's exospheric composition and density should be significantly improved. It is emphasized that probing of Hermean exosphere by ultraviolet spectroscopy (PHEBUS) has several advantages compared to the UV spectrometer of MESSENGER: the extension of the spectral range from 110 nm down to 55 nm provides the capability of observing additional species like He, Ar, N, etc.; using a scanning system allows to greatly improve coverage, vertical sampling rate and trace species detection capability. In the same time, ground-based observations do and most probably will continue to provide original and key information on Mercury's exosphere. As an example, the achievement of long-term program of observations (Potter et al., 2006, 2007), high spectral resolution observations (Killen et al., 1999; Leblanc et al., 2008) and global mapping of Mercury's exosphere (Potter and Morgan, 1990) have already demonstrated the strong links between surface, magnetosphere and exosphere at Mercury.

By performing simultaneous measurements of all detectable exospheric species thanks to its full spectroscopic system, with significant space coverage, due to the use of a dedicated scanning device, and time coverage, due to the low (short period) orbit of Mercury Planetary Orbiter (MPO), PHEBUS will provide four-dimensional maps (altitude, latitude, longitude, time) of Mercury's exosphere. For the first time, the 55–110 nm range will be explored, allowing the measurement of noble gases in conjunction with geochemical studies performed by MPO instruments, and ion species synergistically with ionospheric and magnetospheric studies performed by Mercury Magnetospheric Orbiter (MMO) instruments. Simultaneous measurements of the inner exosphere by PHEBUS and of the outer exosphere by Mercury Sodium Atmospheric Spectral Imager (MSASI) on MMO will provide complementary pictures of exospheric dynamics at various space and time scales. On MPO, the synergistic use of surface composition measurements made by Mercury imaging X-ray spectrometer (MIXS) and escape flux composition made by PHEBUS, together with exospheric composition measurements of PHEBUS and search for exosphere refilling and emitted neutral abundance (SERENA), will allow a robust determination of surface material composition and characterization of surface–exosphere chemical–dynamical cycles.

After a short presentation of key science issues and objectives, a detailed description of the instrument and of its performances will be given. Calibration issues and main observation modes will be then presented. Finally, the main synergies with other instruments of BepiColombo will be described.

2. Key science issues and objectives

2.1. Mercury exospheric system

Fig. 1 displays an example of Mercury's sodium exosphere as it can be observed from Earth ground-based telescope (see Cremonese et al., this issue, 2008 for further details on ground-based observations). The typical high-latitude peaks of sodium emission often observed in Mercury's exosphere (Potter et al., 2006) are visible on both Northern/Southern hemispheres. Several interpretations to these features have been proposed but the most probable and accepted explanations remain the effect of solar wind particles penetrating Mercury's magnetosphere through Earth-type cusp structures, sputtering Mercury's surface and locally increasing the ejection rate of sodium atoms (Milillo et al., this issue, 2008). Another explanation is related to the formation at high latitude of local maxima of surface concentration of sodium atoms due to the recycling of the sodium exospheric particles around Mercury (Ip 1990; Sprague, 1992; Leblanc et al., 2007). Craters or basin have been suggested as potentially inducing exospheric signatures (Sprague et al., 1990, 1997, 1998; Yan et al., 2006), in the same way as it has been suggested that high-latitude craters might permanently trap volatiles as water or sulfur (Harmon et al., 1994). The solar pressure radiation has also been quoted to potentially induce such high-latitude peaks (Potter et al., 2006). More generally, Mercury's exosphere, as observed through its sodium component, appears to be highly asymmetric with local enhancements as just described, dawn to dusk asymmetries (Schleicher et al., 2004) and a long tail in the anti-sunward direction (Potter et al., 2002; Baumgardner et al., 2008).

Thanks to the long-term efforts of Potter et al. (2006), the variation of Mercury's sodium exosphere during an annual cycle is now well constrained. Two peaks in emission brightness at the maximum radial heliocentric velocity of Mercury are observed as expected. The derived total atomic concentration is almost independent of Mercury's distance to the Sun which is surprising knowing that the ejection rates of most of the identified mechanism populating Mercury's exosphere (Fig. 2) have a strong dependency with respect to the heliocentric distance. An

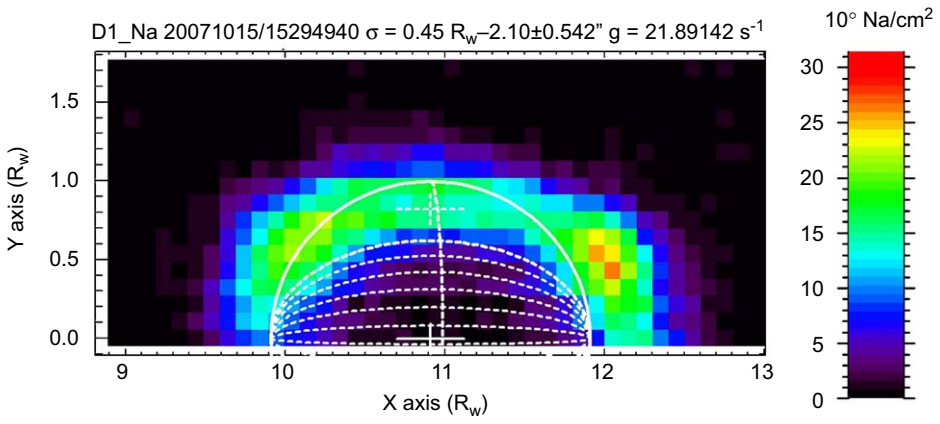

Fig. 1. Reconstructed image of Mercury's sodium exosphere column density (10^9 Na/cm^2) from THEMIS (Canaria island of Tenerife) scan of Mercury's disk. Tip tilt and tracking mode and 220,000 spectral resolution has been used. This observation has been done during the day in October 15, 2007. North/South axis is horizontal and the Sun direction is in the positive y-axis direction. The seeing was equal to 0.4 Mercury's radius. Absolute calibration has been performed using Hapke approach (Leblanc et al., 2006). Optical thin assumption has been considered ($g_{D1} = 22\,s^{-1}$).

explanation suggests that a strong dayside to nightside migration of the volatiles occurs so that the nightside surface being the main reservoir for Mercury's exosphere, the quantity of fresh material available for ejection into Mercury's exosphere reaches a maximum at aphelion because of Mercury's orbital characteristics (Leblanc and Johnson, 2003a). Such an effect may therefore compensate the effect due to the heliocentric distance. Shorter time variations of Mercury's sodium exosphere have been observed. As an example, the high-latitude peaks in sodium emission have been observed to be variable on a time scale of the Earth day (Potter and Morgan, 1990). An increase by a up to a factor 3 of Mercury's total content (Potter et al., 1999) has also been observed and interpreted as produced by the variations of the solar wind flux and UV intensities (Killen et al., 2001).

Clearly, during the last 20 years of study of Mercury's exosphere, it appears that to better understand Mercury's exosphere, we need to be able to constrain the main mechanisms leading to the ejection of surface particles into Mercury's exosphere (Killen and Ip, 1999; Leblanc et al., 2007, Killen et al., 2007), the process of loss by photo-ionization or by direct escape from the surface, the potential recycling by energetic accommodation at the surface or through the magnetosphere and the main sources like meteoroid supply or gardening (Fig. 2).

2.2. Scientific objectives

The core scientific objectives of PHEBUS, oriented toward better understanding the coupled surface–exosphere–magnetosphere system, may be summarized as following:

C1—*Composition and vertical structure*. From vertical scans of the exospheric composition, information about the scale heights of the different species, and their possible variations with altitude denoting the presence of differently generated populations, will be obtained all around the planet, providing information about composition, temperature, release processes, etc.

C2—*Dynamics: day to night active to inactive regions circulation*. The complete local time and latitude coverage will allow to "follow" species from day to night. The significant longitude coverage will allow to get information about local transient active regions and episodic transport in the exosphere.

C3—*Surface release processes and sources*. By measuring the 3-D fields of different species, produced by different release mechanisms (e.g. sodium by thermal desorption and calcium by sputtering), it will be possible to establish maps of the ratios between two specific species used as a signature of a certain release mechanism, and to characterize systematic and/or local (in space and/or time) deviations signing this release mechanism.

C4—*Dynamics of ionized species and their relation with neutral atmosphere*. A few ions are expected to be detected (e.g. Mg^+, S^+, C^+, see Table 1) and mapped as a function of time, together with their source neutral species, which would allow to characterize the formation and dynamics of ions in the exosphere.

C5—*Exosphere–magnetosphere exchange and transport processes*. Characterizing ions and neutrals at the interface with the magnetosphere, synergistically with MMO measurements, should allow to follow planetary ions from their formation region in the exosphere, through the magnetosphere, until escape or re-injection into the exospheric system through the magneto-tail.

C6—*Escape, source-sink balance, geochemical cycles*. Measuring the escape rates of species is of tremendous interest to characterize, synergistically with the results of geochemical instruments (like the X-ray spectrometer), the composition of the eroding regolith. Comparing the escape rate and the exospheric density for each species, it will be

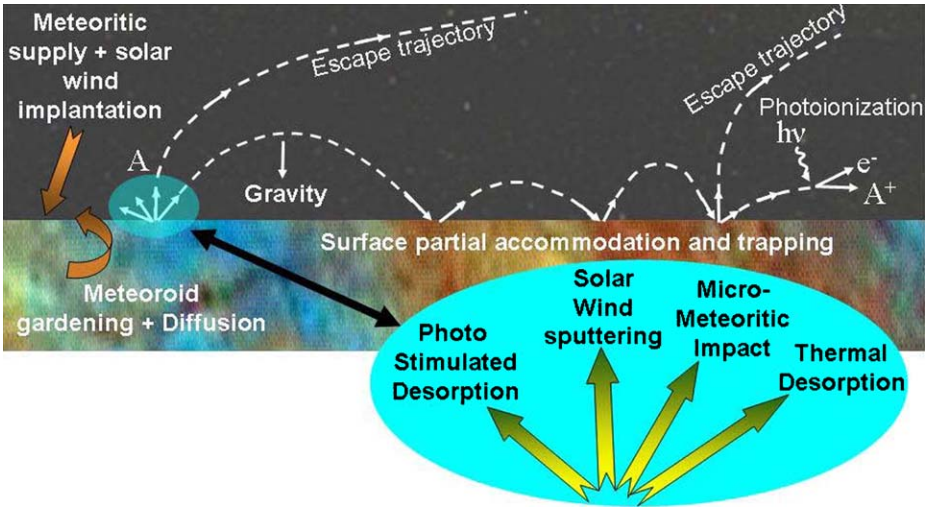

Fig. 2. Main process occurring in Mercury's exosphere, from the ejection from the surface by various processes, the supply of fresh material by meteoritic supply or gardening or by solar wind implantation, the motion of the ejected atoms either along escape or ballistic trajectories up to their trapping into Mercury's surface or their ionization.

Table 1
Classification of the expected species according to their detection difficulty

Detection difficulty	EUV	FUV
Easy (<1 min)	He I, CO, O I, H I, C I, N I	Mg I, Si I, Na I, C I, Fe I, S I, Al I, CO, H I, Ni I, Mg II, O I
Medium (<10 min)	S I, S II, H2, C II	Ca I, H_2, Li I
Hard (<1 h)	Xe I, Ne I	Fe II, OH
Very hard (several hours)	Kr I, Ar I	Al II, K I, Xe I, Ca I
Impossible	Cl I, Si II	Si II

possible to characterize the residence time of this species in the regolith–exosphere system and to constrain recycling to the regolith, and more generally geochemical cycles and source/sink balance. Finally, if noble gases are detected, the present outgassing activity may be characterized, as well as (tentatively) the history of solar wind particle implantation.

C7—*Search for surface ice layers in polar regions*. Some observations on the dark side of Mercury will be dedicated to the search for water ice which may be present in some craters at high latitude. Indeed, some craters close to the poles never receive direct sunlight from the Sun and some water ice brought by comets impacting Mercury may have accumulated there. On the night side of the planet, the main source of Lyman-α radiation is caused by the scattering of solar photons by hydrogen atoms in the interplanetary medium. This creates a glow at 121.6 nm which lits the night side of Mercury. At high ecliptic latitudes, this emission is close to 500 R and varies by one or two hundred Rayleighs with the solar cycle. If present, water ice will be detected by variations of the surface albedo at 121.6 nm. Assuming that the mean UV albedo of Mercury is close to the value of the UV albedo of the Moon, that is around 4%, we should get a signal around 20 R. For water ice, the albedo at 121.6 nm is close to 2% (Hendrix and Hansen, 2008). In that case, we should see a decrease of the signal by a factor of two, that is 10 R in that case, when the line-of-sight (LOS) reaches a surface covered with water ice. The actual observations may be more complicated according to the actual UV albedo value of the surface. A similar idea is being used on the Moon by the Lyman Alpha Mapping Project (LAMP) instrument (Stern et al., 2004) on the Lunar Reconnaissance Orbiter to try and find the presence of water ice in lunar craters.

Two additional objectives relative to heliospheric and solar physics deserve to be mentioned.

A1—*Interaction of interstellar gas with solar environment*. Sky background measurements with PHEBUS at the resonance lines of H, He, He^+ (121.6, 58.4 and 30.4 nm) can provide new diagnostics on the interstellar gas in the heliosphere and its interaction with the solar wind, due to the unprecedented vantage points at small solar distance.

A2—*Solar corona*. The emission lines of the solar corona will be observed in the twilight mode, when the sun is occulted by the Hermean disk. Provided the sun is sufficiently close to the Hermean disk, coronal lines will be observed, superimposed with Mercury exospheric lines. Scientific objectives in this field have still to be investigated.

2.3. Measurement objectives and requirements

The main measurement objectives of PHEBUS are:

1. To detect new species, including metallic species (Si, Mg, Fe, etc.), atoms (C, N, S, etc.), molecules and radicals (H_2O, H_2, OH, CO), noble gases (Ar, Ne), ions (He^+, Na^+, Mg^+, etc.), in addition to already detected species (Na, K, Ca, O, H, He).
2. To measure an average exosphere (number densities of constituents, vertical structure), with as much as possible species monitored together, at different positions of Mercury around the Sun. Averaging over 1/8 of Mercury's year, that is on a time scale of 10 Earth days, is appropriate.
3. To measure sharp local and temporal variations of the exosphere content (time scale: less than a few hours), at specific times and places of interest.
4. To search for albedo variations of Mercury's nightside surface, lighted by the interplanetary H Ly-α glow, at 121.6 nm, in order to exhibit possible signatures of surface ice layers (H_2O, SO_2, N_2, CO_2, etc.) in high-latitude polar craters, and any other signature of interest on the nightside.

The required accuracy and precision on measured abundances are 30%. Due to the large natural variability of Mercury exospheric densities, there is no stringent requirement on the precision, which can be taken equal to the accuracy. The required vertical spatial resolution is 15 km (the half of the lowest scale height, that is 30 km for K) in the range from 0 to 400 km altitude. The best compromise in terms of spectral resolution is 1 nm for the extreme ultra-violet (EUV) range (55–155 nm), 1.5 nm for the far ultra-violet (FUV) range (145–315 nm), potentially allowing to measure most of the expected elements (see Table 1). The sensitivity is 0.1 ct/s/R, and the dynamics may reach 4–5 orders of magnitude for spectrally isolated lines. Only a few interesting lines are outside the EUV–FUV range of PHEBUS, mainly He^+ and Na^+ at short wavelength (30–40 nm), and K and Ca at long wavelength (400–420 nm), although some weak Ca lines can be expected to be present, and marginally detectable, in the FUV range. A specific near ultra-violet (NUV) detector is implemented in PHEBUS to measure K and Ca, which are important species, produced by different processes at the surface of Mercury. No specific detector is implemented for very short wavelengths, but interesting ions can be detected in the FUV (Mg^+) and EUV (S^+, C^+) ranges of PHEBUS.

A simple global analysis shows that a significant fraction of the exosphere has to be mapped at least every 1/8 of one Mercury's year (that is every 10 Earth day), in order to

catch and correctly sample North/South and East/West asymmetries of the exosphere, as observed from Earth for Na. A complete coverage in latitude is expected during this typical sampling period, thanks to the MPO polar orbit. The scientific reasons to look for a wide coverage of Mercury's exosphere at different heliocentric Mercury's position is that significant North/South and East/West asymmetries of the Na exosphere have been observed (Sprague et al., 1997; Potter et al., 1999). Such structures are very important in order to understand the mechanisms at the exosphere's origin and the behavior of the exosphere in its environment. Moreover Leblanc and Johnson (2003a) have shown that the total content of the Na exosphere should greatly vary with respect to Mercury's heliocentric position due to the variation of Mercury's rotation around the Sun (this variation leads to important variation of the speed with which Mercury's surfaces enriched in volatiles reach the dayside). Recently, Potter et al. (2007) have derived from 6 years of observation the annual variation of the total content of the Na exosphere displaying a maximum at Mercury's aphelion as predicted.

The one degree-of-freedom pointing device of PHEBUS, with a scanning capability within the orbit plane, achieves a significant latitude/altitude sampling and to satisfy the mapping coverage requirement, as shown by the results of a numerical simulation. Fig. 3 shows the region of Mercury's exosphere which will be observed by PHEBUS during 10 successive Earth days (for four regions of True Anomaly Angle, TAA, i.e., at four Mercury's positions around the Sun).

Fig. 3 shows that for some heliocentric position of Mercury a coverage of 1/5 of Mercury exosphere can be obtained (at the perihelion where Mercury angular velocity is the largest) but that in other regions, the coverage is less good (at the aphelion where Mercury angular velocity is the smallest). Even the use of a two degree-of-freedom scanning system would not allow a full coverage of the Hermean exosphere, and the proposed system is therefore a good compromise, allowing to achieve a substantial coverage with a reasonably simple (and light) scanning system.

3. Instrument general design

3.1. Schematic view

3.1.1. Instrument concept

PHEBUS is a double spectrometer for the Extreme Ultraviolet range (55–155 nm) and the Far Ultraviolet range (145–315 nm) with an extension for two extra visible emission lines at 404 and 422 nm.

The spectrum detection is based on the photon counting method and is realized using micro-channel plate (MCP) detectors coupled with Resistive Anode Encoder (RAE). Typical photocathodes are Cesium Iodide (CsI) or Potassium Bromure (KBr) for the EUV range, Cesium Telluride (CsTe) for the FUV range. The main advantages of these MCP + RAE detectors are their very high sensitivity mainly due to a very low dark current. Photon counting is then easily achievable at typical experiment temperature (−20 °C/ + 40 °C), avoiding mass and power

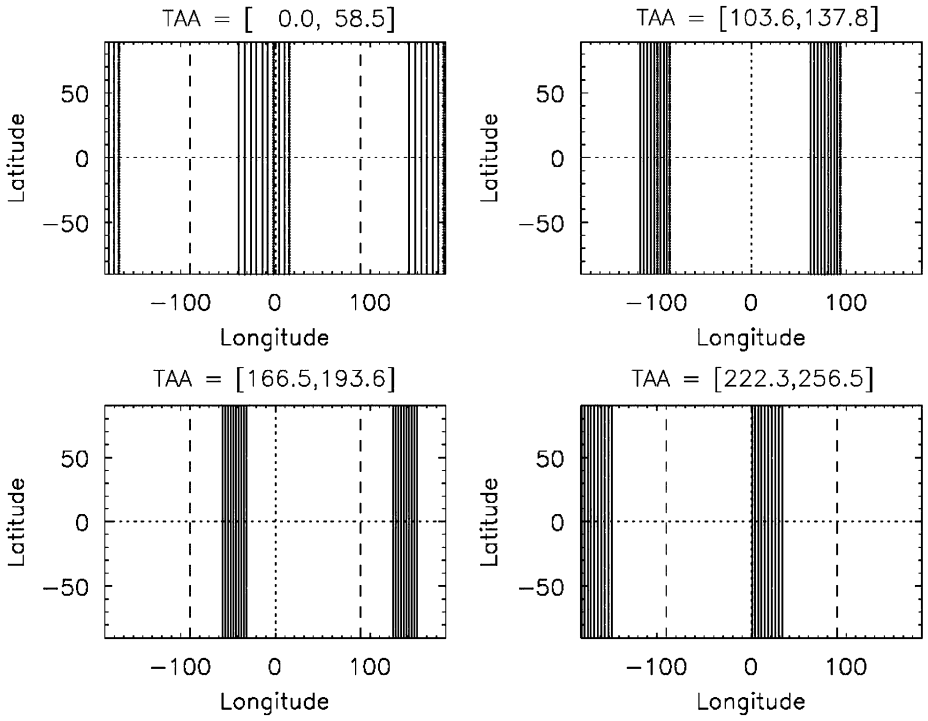

Fig. 3. Longitude and latitude of the LOS coverage of PHEBUS during 10 successive Earth's days at different position of Mercury. The center of each panel is centered on Mercury's subsolar point, Mercury dayside being between the two horizontal dashed lines.

expensive devices to cool the detectors. Seven orders of magnitude for the detection are then a typical value and offer the monitoring of a wide range of emission lines.

Extra visible lines are monitored using low noise photomultipliers (PMs) with bi-alkali photocathodes also used in photon counting mode.

In order to prevent sensitivity losses which are critical in UV ranges, a minimum number of reflections is guaranteed inside the instrument using only an off-axis parabola and a set of holographic gratings. The off-axis parabola is movable thanks to a rotating mechanism and will take the light from the exosphere above the limb onto the entrance slit of the spectrometers. As long-term orbital stability may not be guaranteed, this scanning mirror is required:

- to maintain the instrument LOS close to the limb during long integration time sequences,
- to make the search and monitoring geometry less dependent on orbit,
- to extend the vertical range of scanning.

The main advantage of this concept is the optimization of the optical layout which allows, on one hand a compact and relatively light instrument, on the other hand a very versatile instrument due to the rotating entrance mirror. The instrument is then independent of the spacecraft on an observation point of view, avoiding spacecraft slew for specific pointing request.

Limitations however exist. Due to the very high sensitivity of the MCP + RAE detectors, the instrument is only devoted to the very faint emissions. A big effort must be then taken to avoid direct illumination of the detectors by strong light sources such as Sun or the reflective surface of the observed planet. This effort induces at instrument level the need of several baffles which increase the mass. Another point is the high sensitivity of the instrument to the dust contamination during the integration which can induce straylight, but also to the molecular contamination which can induce absorption especially in UV. Finally, due to the degrading effect of the moisture and the air on the UV photocathodes, especially EUV ones, and because UV light does not propagate through windows below 115 nm, the EUV detector needs a mechanism to open its window once in space and its sensitive area (photocathode + MCP + RAE) has to be maintained under vacuum during the whole integration life of the instrument on ground (vacuum level around 10^{-2} mbar). A specific pumping device is then permanently needed for the EUV detector and has to be removed as late as possible before the launch. It means also that adjustments and calibration of the EUV part of the instrument must be realized under vacuum only, with windowless sources.

3.1.2. Instrument subsystems

The instrument consists of several subsystems all included inside a single box. An entrance baffle allows straylight rejection outside a defined guard angle ($\sim 8^\circ$). In order to survive to the expected hot environment around Mercury outside the spacecraft, the baffle will be protected by high-temperature multi-layer insulation (HT-MLI). This baffle is mounted on the rotating mechanism which has a $\sim 0.1^\circ$ pointing accuracy. This mechanism is developed by the Space Institute of Moscow (IKI). At the output of the baffle, the scanning mirror takes the light from the observed scene onto the entrance slit of the spectrometers. This slit can be removed for star observations periodically required for absolute calibrations of the instrument. The slit is then mounted on a two positions actuator. Two holographic gratings are accommodated after the slit and share it. These gratings define the EUV and FUV spectrometers with a typical resolution of 1 and 1.5 nm, respectively. In order to work under 115 nm, the EUV detector works without window, whereas the FUV one is sealed. These two UV detectors are developed by the University of Tokyo (Department of Earth and Planetary Science). Due to the size of the FUV detector housing, it is not possible to accommodate the two PMs required for the extra visible line monitoring directly at the focal point of the two wavelengths of interest. A double aperture deviation prism and two spherical mirrors take then the light at 404 and 422 nm in front of the FUV detector towards the PMs. On an electrical point of view, all the subsystems work together under the authority of a central data processing unit (DPU) and are supplied by a power conversion board which transforms the 28 V from the spacecraft into all the needed secondary voltages.

All these optical and mechanical subsystems are accommodated together inside a mechanical and structural part composed of two main pieces. The first one called the main structure holds all the massive subsystems which are the rotating mechanism, both EUV and FUV detectors, the two PMs with their electronics, the DPU and power boards. The second structure is a light cover which only holds the gratings and a small nitrogen flushing system.

Two other extra subsystems are linked to the instrument. The first one is a vacuum device operated permanently during ground operation for the EUV detector (but removed before launch so considered as a Red Tag Item), the second one is a parking bracket attached to the spacecraft which has to protect the entrance baffle aperture during non-operating period.

The PHEBUS block diagram and general overview are shown in Figs. 4 and 5.

3.2. Optical design

The optical configuration of PHEBUS can be divided into two relatively independent parts.

The entrance of the system is called the Collecting Part. It is constituted by the entrance baffle (whose exit diaphragm is in fact the entrance pupil of the global instrument), the entrance parabolic mirror, and the entrance slit. This part determines the characteristics of

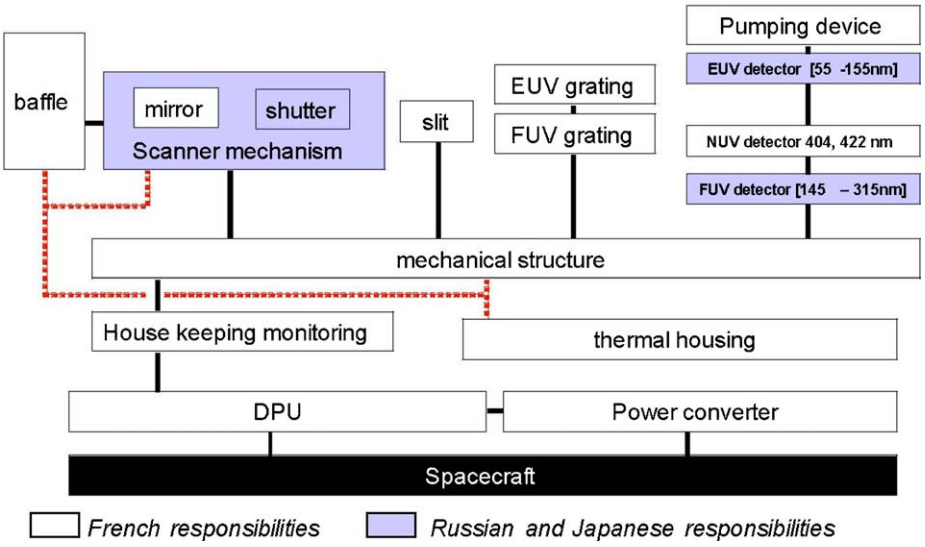

Fig. 4. PHEBUS block diagram (without parking bracket).

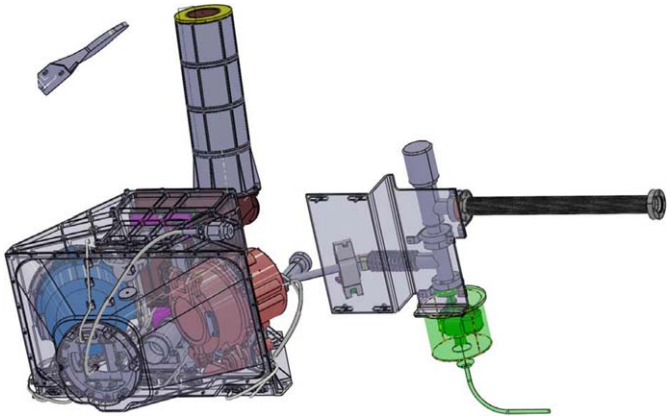

Fig. 5. PHEBUS general overview (from left to right: parking bracket, main unit, pumping device).

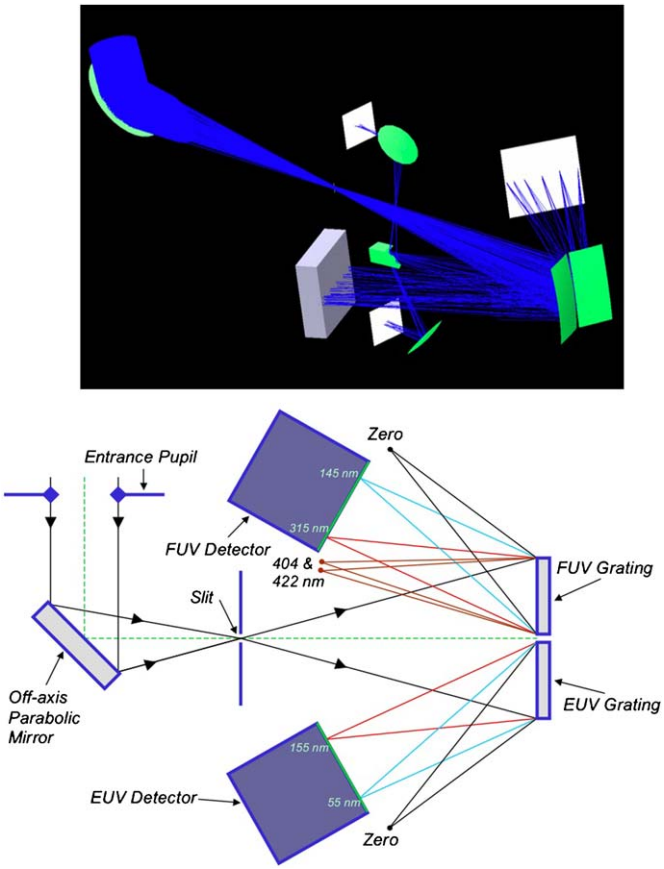

Fig. 6. PHEBUS optical layout.

the field of view, the LOS, and the point source image quality.

The other section of the system is the Spectrometer Part strictly speaking, with the entrance slit, the gratings, and the detectors (including NUV path). This part mainly determines the spectral resolution of the instrument.

The whole optical system has been optimized with the help of the ZEMAX-ray-tracing software (Fig. 6): the keys of the optimization are the gratings, characterized by the position of their construction points. The goal of the optimization is to obtain the best balance between spectral resolution and photometric performances, according to the scientific requirements, that is the detection of a certain number of important constituents (see Table 1). The required spectral resolution is 1 nm for EUV and 1.5 nm for FUV. These values are to be compared with the result of the optimization: the full-width at half-maximum of one line is about 0.5 nm on EUV, and 0.8 nm on FUV. Furthermore, the full-width at 1% of maximum (FW1%) is about 0.9 nm on EUV, and 1.5 nm on FUV (these calculated values do not include any spreading effects due to scattering by gratings).

4. Instrument description

4.1. Entrance baffle

The PHEBUS entrance baffle has the difficult task to avoid direct light inside the instrument due to bright sources outside a defined guard angle. In the case of PHEBUS, the main bright source to avoid inside the instrument is the surface of Mercury on the day side. For angles bigger than the defined guard angle, the light coming from this unwanted source reaches however the inner part of the baffle. The other purpose of this subsystem is in this case to attenuate as much as possible the induced straylight inside the instrument due to multiple reflection and diffusion on its internal surfaces. If the attenuation is high enough, it will be then possible to perform exospheric observations as close as the guard angle value from the Mercury illuminated surface. On a design point of view, the baffle geometry is fully dependant on a combination of optical constraints:

- the instrument guard angle ($\sim 8^\circ$),
- the instrument field of view (IFOV) ($\sim 2^\circ \times 0.1^\circ$),
- the instrument collecting surface ($\sim 500\,mm^2$),
- the stable illumination pattern on the gratings when the rotating mechanism is moving.

To fulfill these four optical constraints, the PHEBUS baffle is then a single aperture 4 stages–5 diaphragms baffle (Fig. 7). Its length is 210 mm, its external diameter is about 60 mm, and it is rotationally symmetric. The exit diaphragm of the baffle is the entrance pupil of the instrument, with a diameter of 25.4 mm.

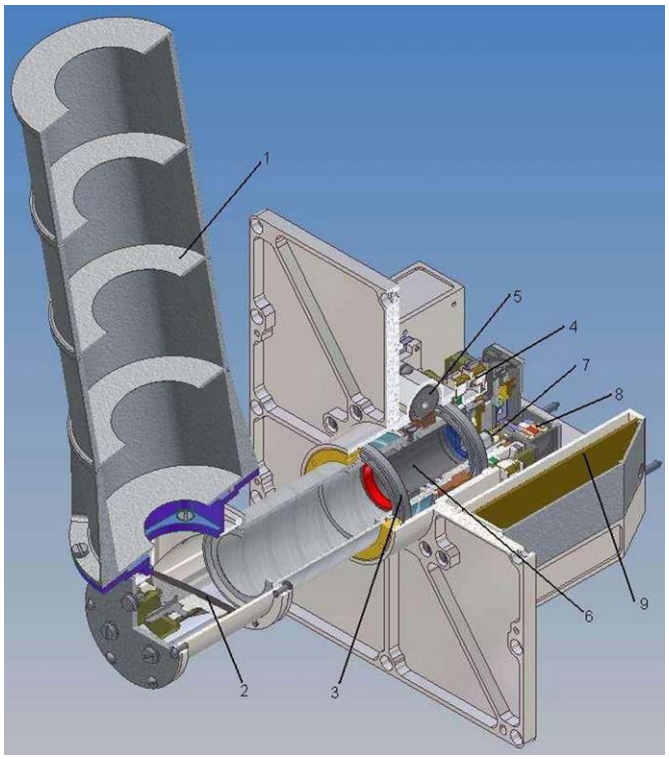

Fig. 7. The 3D drawing of the scanner mechanism. The main elements are: 1—entry baffle; 2—scanner head with parabolic mirror; 3—ball bearings; 4—rotation angle gauge; 5—driving mechanism; 6—internal baffle; 7—light detector (photometer); 8—shutter; 9—electronics.

The requested light attenuation (defined at 10^6) for sources external to the guard angle has no real impact on the geometry, but on the inner surfaces quality. Two parameters have to be considered: the total integrated scatter (TIS) factor for flat surfaces, and the edges size for the diaphragms. Black coating with very low TIS has been selected (typical value $\sim 1\%$), and the diaphragms are optically polished before the black treatment to obtain typical values of edges size around 20 μm. Last constraints for this subsystem are mechanical and thermal ones. Assuming that the baffle is mounted on a rotating mechanism, its mass has to be as low as possible. On a thermal point of view, and even if the main part of the baffle will be protected by HT-MLI due to IR and Albedo fluxes coming from the planet, the baffle will be able to reach very high temperatures ($\sim 200\,^\circ C$) near perihelion and aphelion. To save mass and avoid thermal constraints, the baseline is then to propose a full aluminum baffle and to perform a laser welding assembly of the stages. The target mass is 120 g (without HT-MLI).

4.2. Entrance mirror

The entrance mirror is positioned just after the baffle exit (which defines the instrument pupil) and is accommodated inside the rotating mechanism. This subsystem has to focus the light beam on the spectrometers entrance slit. The proposed optical shape is then an off-axis paraboloid, with an effective focal length of 170 mm, working at an angle of 100°.

For nominal exospheric observations, the main parameter of this mirror is its reflective surface roughness quality (specified at 0.5 nm RMS which corresponds to a superpolished quality) to avoid as much as possible straylight inside the instrument coming from the baffle, while for star calibrations it is its surface figure quality (shape error specified lower than 200 nm RMS @633 nm) in order to limit the star image size within the focal plane.

To be reflective enough in UV ranges, especially the EUV one, the mirror material is silicon carbide (SiC). The substrate is obtained using sintered SiC and then a SiC layer is deposited by chemical vapor deposition (CVD process) on the optical surface. This is this CVD layer which is finally polished using a combination of different techniques. The SiC solution offers a homogeneous mirror in terms of material and thermal behavior, which is very important in the PHEBUS case because the mirror is accommodated on the outside part of the spacecraft so within a difficult thermal environment. However, because the rotating mechanism is made of aluminum, the SiC mirror is thermally decoupled from this mechanism using a Titanium or Invar tripod. The total mass (mirror + tripod) is 25 g.

4.3. Scanner mechanism

The main function of the PHEBUS scanner mechanism is to point spectrometer's LOS to the desired location. Using the orbital motion of the MPO satellite, a one-dimensional rotating scanner allowing full 360° rotation provides the desired coverage of the Mercury exosphere, to fulfill the scientific objectives of PHEBUS. Also, the scanner mechanism is equipped with a photometer to monitor the luminosity level, and with a high-speed shutter to protect the detectors of the spectrometer against inadmissible levels of light exposure.

A 3D view of the scanner mechanism is presented in Fig. 7. The main elements of the mechanism are:

- entry baffle,
- scanner head with parabolic mirror,
- ball bearings,
- rotation angle gauge,
- driving mechanism,
- internal baffle,
- light detector (photometer),
- shutter,
- electronics.

Scanning is performed by a rotation of the scanner head around the optical axis of the spectrometer traversing its slit. The scanner head hosts the off-axis parabolic mirror, serving as the entry telescope of the instrument and carries the entrance baffle, forming the entry aperture.

The scanner head is a termination of a hollow shaft centered on the optical axis, and mounted with a help of two large diameter ball bearings. The shaft is driven by a stepping motor via a worm drive with the reduction ratio of 1:29. The ball bearings and the gearing parts are lubricated with vacuum silicon lubricant VNIINP-274, having a guaranteed operation time of 900 h. To protect the optical elements of the spectrometer from lubricant outgassing products dedicated labyrinth gaskets with additional reservoirs are employed.

A rotary position detector, or angle gauge, serves to account for eventual slack in the gearing. The sine–cosine gauge employs permanent ring magnet and two Hall-effect devices located at 90°. One additional Hall-effect device is used to determine the home position of the scanner. The Hall-effect devices for the angle gauge have been widely used in Russian space instrumentation, in particular such gauge is working in the scanning mechanism of Observatoire pour la Minéralogie, l'Eau, les Glaces et l'Activité (OMEGA) mapping spectrometer on Mars Express during more than 4 years.

To protect the UV detectors from an occasional excessive illumination, the optical path can be blocked by a blend located in the proximity of the spectrometer slit. The blend is activated by an electromagnetic actuator, either in automatic mode or by a telecommand. In the automatic mode two photometers (Hamamatsu photodiodes) located before the blend monitor the intensity of light, and when a preselected threshold is achieved, the shutter is automatically closed. The position of the shutter is monitored with a help of two Hall sensors.

Table 2
Main characteristics of the scanner mechanism

Rotation range	360°
Scanning rate	4° per minute
Maximal rotation speed	5° per s
Accuracy of angle measurement	0.1°
FOV	1° × 1°
Unobscured diameter of the parabolic mirror	33 mm
Focal length of the mirror	170 mm
Mass	1100 g
Working temperature range	±60 °C
Electrical interface	RS-422 at 115,200 bits/s
Guaranteed operational lifetime	900 h

The thermal regime of the scanner mechanism is provided with passive means. The external baffle scanner head are closed by multi-layer insulation (MLI), the flange and a part of the scanner shaft are below the MLI of the spacecraft. The baffle and the scanner head which could become hot under certain conditions are thermally isolated from the rest of the instrument by means of the long thin-walled shaft. The main and most sensitive parts of the scanner and the spectrometer are located inside the spacecraft and will have a temperature close to the temperature of the spacecraft (~60 °C).

The basic constructive element of the scanner mechanism is the flange with which the scanner is attached to the spectrometer. The flange carries also the driving mechanism and the electronics.

The scanner field-programmable gate array (FPGA)-based electronics is designed on the principle of full redundancy and includes three PCBs. It provides communication with the electronic block of PHEBUS, controls the stepping motor and shutter actuator, and processes signals from the photometers and Hall devices.

The main characteristics of the scanner mechanism are given in Table 2.

4.4. Slit

The slit is accommodated at the focal plane of the entrance mirror, and it defines the required IFOV for exospheric observations and is part of the instrument performance in term of spectral resolution. Considering the entrance mirror effective focal length of 170 mm and a slit rectangular aperture of around 5.6 mm × 0.28 mm, the IFOV is ~1.9 × 0.095°. Considering the orientation of PHEBUS inside the spacecraft, the large dimension of the field of view is then parallel to the limb in order to accurately sample a vertical scan of the exosphere.

For star observations, and because it is necessary to catch more than 90% of the star flux to perform absolute

calibrations, the slit has to be removed from the focal plane. Due to the entrance mirror aberrations, the star image size is actually bigger than the slit size. The slit is therefore mounted on a rotating arm which is linked to a two positions actuator. Such a device has already been used for previous UV spectrometers on board Mars Express and Venus Express missions. The total mass of the slit assembly is around 80 g.

4.5. Gratings

The two gratings of the PHEBUS instrument are aberration corrected holographic gratings. This technology has two main advantages. First, the total number of reflections must be as small as possible in order to avoid reflection losses in the UV range, so it is very interesting to use only one component to spread and focus the spectrum from the slit onto the detector. But with only one component, optical aberrations cannot be corrected on the flat surface of the detector, so a classical constant-line spacing grating is not sufficient to reach the spectral resolution requirements. Holographic gratings are especially dedicated to aberrations compensation and can be optimized to correct the optical configuration, whereas ruled gratings correction capabilities are very limited.

The other main advantage of using holographic gratings is their very low surface micro-roughness, which induces a very low level of scattered straylight compared to ruled gratings. Indeed, a low level of scattering is required in order to perceive some faint emission lines close to some bright other lines.

The two gratings are characterized by their spherical radius of curvature and by the position of their recording points. EUV and FUV gratings have been forced to the same curvature (~170 mm) to simplify manufacturing tools. The mean groove density is ~1600 g/mm for the FUV and ~2700 g/mm for the EUV. Groove profile is laminar ion-etched optimized for the respective spectral range. Atomic force microscopy (AFM) measurements on real prototypes show a micro-roughness of about 1 nm RMS. The absolute efficiency can be deduced from AFM measurement of the groove profile via electromagnetic theory software codes: about 6% for EUV and 13% for FUV.

The gratings are made of aluminum with a reflective platinum coating. Their active area size is 42 mm × 15 mm. Since the two gratings share the same entrance slit, a big effort on their accommodation is needed in order to reduce as much as possible the gap between the two useful areas, where a non-negligible amount of light is lost.

4.6. FUV and EUV detectors

4.6.1. FUV detector

FUV detector consists of an input window made of MgF_2, MCPs, position-sensitive anode, electronics and a high voltage module. The MCP assembly is vacuum sealed by the ceramic body and the input window. Cesium Telluride (CsTe) is coated on the backside of the input window as a photocathode. It has a high efficiency in the FUV range (120–330 nm). The FUV detector uses 5-stage MCPs (V&Z stack) for electron amplification. Each MCP has a circular shape with an active area of 13.9 cm^2, bias angle of 8°, and 12 μm pore with a L/D ratio (ratio of length to pore diameter) equal to 40:1 with a total resistance of 125 MΩ. The front two (V-stack) and the other three (Z-stack) MCPs are placed in direct contact as a back-to-back stack. An important indicator of the MCP stack performance is the pulse height distribution on a single photon event. Fig. 8 shows a pulse height distribution with −3.2 kV applied at the MCP face. Pulse height ratio (PHR: width of the pulse height distribution) is narrower by 70% than we would expect from a 3-stage MCP stack. Behind MCP stacks, the RAE is placed to determine the position of photon injection. Electron cloud emitted from Z-stack MCPs consists of an order of 10^7 electrons and impinges on RAE. Electron cloud is divided toward four electrodes at the corners in reverse proportional to the distance to them. RAE has an effective area of 20 mm × 40 mm. Electronics digitalizes 512 × 512 pixels.

Signal at each electrode is amplified by A-250 (AMPTEK). Pulse-shaper (A-206) further amplifies the signal and recognizes the event with a threshold level. When A-206 identifies significant signal level, it sends "ready" signal to the main electronics. PH-300 holds the signal peak and ADC digitalizes the height of the signal. Main electronics computes the position. The image linearity and resolution was measured by imaging an array of pinholes in a metal mask illuminated by a beam, as shown in Fig. 9a. The ion-etching mask was placed at 8.3 mm off from the input face. Fig. 9b indicates that a 80 μm resolution is achieved. The expected mass of the FUV detector is around 1 kg.

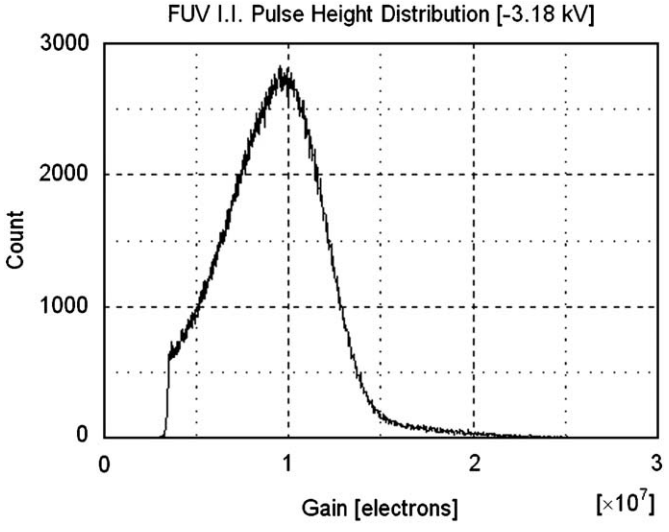

Fig. 8. Pulse height distribution with −3.0 kV applied. The pulse height ration is about 70%.

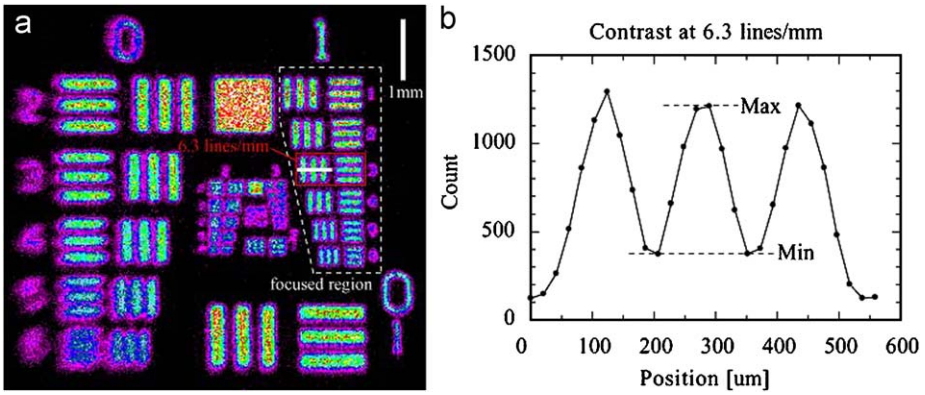

Fig. 9. (a) A test target image obtained by the FUV detector breadboard. The series of patterns encircled by dotted line are well focused. (b) A cross-section profile of the image (a) taken along the white line at 6.3 lines/mm. The contrast at 6.3 lines/mm is 0.53.

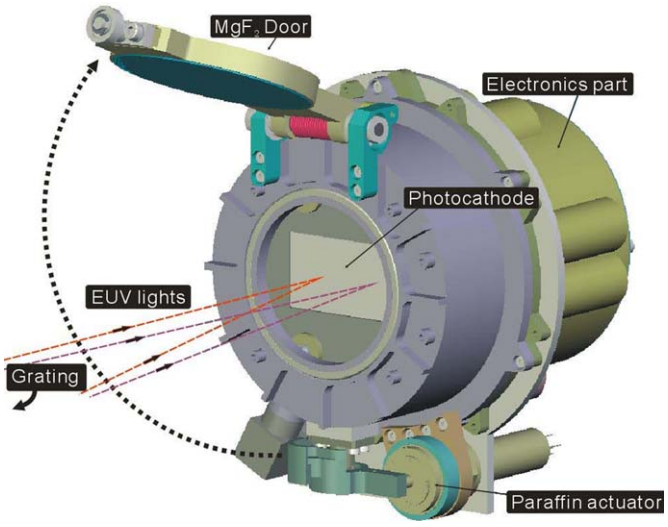

Fig. 10. EUV detector.

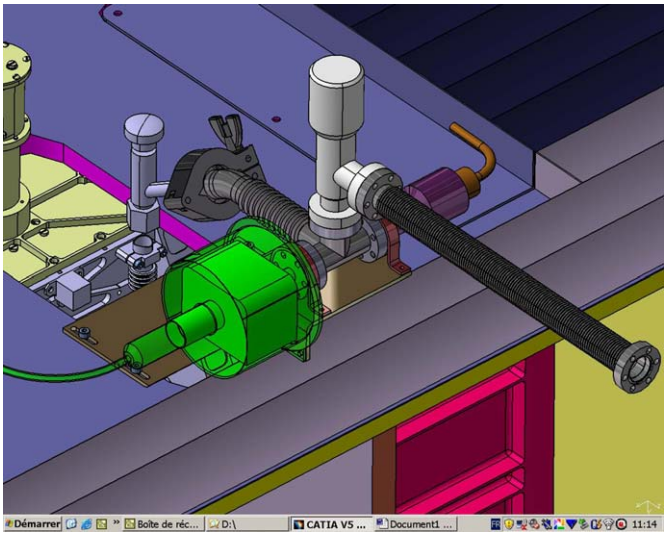

Fig. 11. PHEBUS vacuum pumping device.

4.6.2. EUV detector

A 5-stage MCP coated with CsI is located at the focal plane of the EUV grating. The MCP dimension and principle are the same as the FUV one. Except the following points, EUV detector is designed similarly to the FUV detector. CsI is the nominal photocathode to be used (KBr is an alternative solution) and is very sensitive to the moisture. The moisture reduces the quantum efficiency of the CsI. Therefore, the MCPs are kept in a vacuum chamber with a movable MgF_2 window. After a paraffin actuator activation, MgF_2 window can be opened and EUV detector can detect the input radiation from the grating at wavelength <115 nm. The expected mass of the EUV detector is 1.1 kg. A view of the EUV detector is shown in Fig. 10.

4.7. EUV detector vacuum system

Due to the spectral range of the EUV detector (<115 nm which is the MgF_2 transmission limit), this subsystem needs to work in space without window, with a photocathode directly in contact with photons. This request means that this detector is equipped with a removable window, which will be opened on ground only during calibration activities and opened definitively in space several days or weeks after the launch. Due to the degrading effect of the moisture and the air on the photocathode, the sensitive area (photocathode + MCP + RAE) of this detector needs to be under vacuum ($\sim 10^{-2}$ mbar) from the detector manufacturing up to the launch. A vacuum pumping device is then attached permanently to the instrument and will be mounted on the spacecraft after instrument delivery (Fig. 11). It will be removed as late as possible before the launch. The device uses a miniature ion pump (2 l/s) which works permanently. This device will be removed for instrument and spacecraft test periods (vacuum, vibration). It shall then allow multiple connections. In order to be able to initiate the ion pump, a turbomolecular pump will be installed in the vicinity of the vacuum device. The device integrates then two valves (one to disconnect the entire device from

the instrument, the other one to disconnect the turbomolecular pump from the device), the miniature ion pump protected inside a magnetic shield and a miniature vacuum gauge.

4.8. NUV detector

The NUV detector is composed of two separate detectors, the first one for the potassium (K) emission line monitoring at 404.7 nm and the other one for the calcium (Ca) emission line monitoring at 422.8 nm. For both lines, the expected light flux in front of the detectors is within the range 100–10,000 photons/s (after reflections on the entrance mirror, the gratings and the NUV optics in front of the FUV detector). Considering this low light level, the detectors are based on low noise photo-multiplier tubes (PMT) used in photon counting mode. The selected PMs have the following characteristics: quartz window, ruggedized, low profile, 25 mm (1 in) diameter, low noise bi-alkali photocathode (sensitive between 300 and 650 nm), up to 70 °C operation, 10 stage, head-on type. The typical dark current value of these PMs is 10 counts/s at 25 °C, which allows an interesting signal-to-noise ratio. A magnetic shield made of mumetal is accommodated around the PMs to protect them from the magnetic environment (mainly the one generated by the rotating mechanism). Due to the heavy density of this material, it will also offer an interesting protection against radiations. Two electrical boards are accommodated as close as possible to each tube, one for the high voltage supply (~1000 V) and the other one for the voltage divider and the pre-amplifying functions. The total mass of one channel is 225 g.

4.9. Mechanical structure

The mechanical structure of PHEBUS is mainly divided in two parts. The first one is called the main structure and holds all the massive subsystems of the instrument which are: the rotating mechanism, the slit assembly, EUV and FUV detectors, NUV detectors, the DPU and the power boards. In order to gain mass on this main structure, it has been decided to propose an innovative design. The previous UV spectrometer onboard Mars Express and Venus Express missions was actually based on an "optical bench" concept, which means a flat structural part with all the subsystems accommodated on this surface. For PHEBUS, due to the strong mass constraints with respect to the number of subsystems to accommodate, the main structure is a complete 3D design piece made of aluminum around the subsystems. Advantages are quite evident: stiffness, mass improvement, decreases of the inertia, integrated mass around the subsystems which provide an improved radiation shielding, machining precision achievable, thermal conductivity and diffusivity increases. The mass of this main structure remains around 750 g to hold more than 5 kg. Limitations however exist, the main one being the complete optimization of this main structure around the subsystems. If a subsystem evolves, the main structure needs also to be modified. Interface and envelope of each subsystem have been then defined very early in the project.

The second part of the structure is a cover which only holds the gratings assembly and a small flushing system. A first prototype has been manufactured in carbon-epoxide material (with low outgassing properties) with a mass of 120 g. An aluminum back-up solution using welded sheets is under investigation.

4.10. Mechanical and thermal design

From a mechanical point of view, the PHEBUS design is built around the optical configuration, in order to optimize its mass and size. The mechanical design is realized with the CATIA V5 software. The PHEBUS vibration behavior is then validated thanks to PATRAN and NASTRAN software. Preliminary results show a complete structure stiff enough, according to the interface vibration levels provided by ESA.

From a thermal point of view, the PHEBUS specificity is to have a part outside the spacecraft, which will be subjected to the external thermal environment, and a part inside the spacecraft, which will be subjected to the internal one (Fig. 12). This is the reason why the PHEBUS thermal model is divided into two models: one for the external part, and the other for the internal one. Compliant with ESA requirements, the PHEBUS thermal model is developed with ESARAD and ESATAN software. For the external part, the spacecraft (radiator side) is taken into account in the thermal model in order to consider multi-reflection phenomena. The PHEBUS entrance baffle

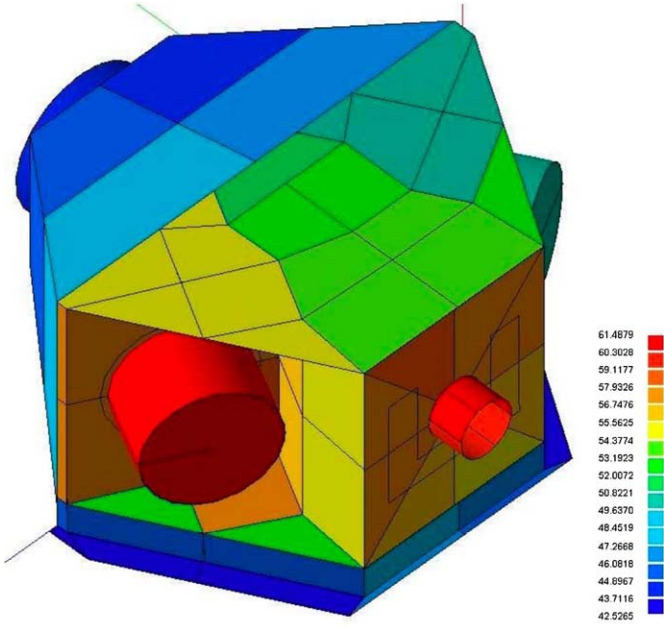

Fig. 12. PHEBUS internal part thermal model (Mercury at Perihelion, MPO at 1200 s from the Periherm).

will be protected from the solar and Mercury radiations thanks to a high-temperature MLI.

Concerning the thermal control of the internal part of the instrument, PHEBUS will be black coated as far as possible, in order for the outer side to radiate inside the spacecraft, and for the inner side to be the most efficient from an optical point of view (black coatings will avoid straylight). Moreover, heaters will be set on the PHEBUS optical gratings to clean them during the cruise. Preliminary results show, for the worst hot case (Mercury at Perihelion), that the baffle will bring back a bit less than 4 W inside the spacecraft (it will depend on the HT-MLI efficiency). Despite the MLI protection, the baffle temperature might reach 200 °C if it sees the Sun. Moreover, with a dissipation considering that PHEBUS fully works, the main structure temperatures go from 42.5 to 59 °C (see Fig. 12).

4.11. Electrical design

On an electrical point of view, PHEBUS subsystems are organized around three main functions: a DPU, a Subsystems and Housekeeping Interface board (HK-IF) and a Power Distribution Unit (PWR) (see Fig. 13).

The DPU is the management unit in charge of the following subfunctions:

- Telemetry/Telecommand Interface: communication between instrument and spacecraft, through a serial interface (Spacewire, LVDS).
- SubSystems Interfaces (Detectors, Front End Mechanism, etc.): subsystems control and monitoring (Synchronous or RS422, LVDS).
- Central Processing Unit:
  - Operational Modes Management
  - Electronic Management (Subsystems ON/OFF, Reset, etc.)
  - Data Processing
  - Bus Memory Control
  - TC/housekeeping (HK) Management.
- Data storage:
  - Program Boot Memory
  - Current Program Memory
  - Data Memories (HK data, Detectors data).
- Power Interface.

The subsystems and HK-IF board has the following function:

- PHEBUS experiment analog telemetry management,
- NUV/Slit Subsystems command and control.

This HK-IF board interfaces with:

- the PHEBUS Power Distribution Unit for its power supplying,
- the DPU via digital FPGA interfaces for TMTC of the HK-IF unit,
- the PHEBUS subsystems via analog interfaces for their control and monitoring (NUV/Slit) and housekeeping (Scanner).

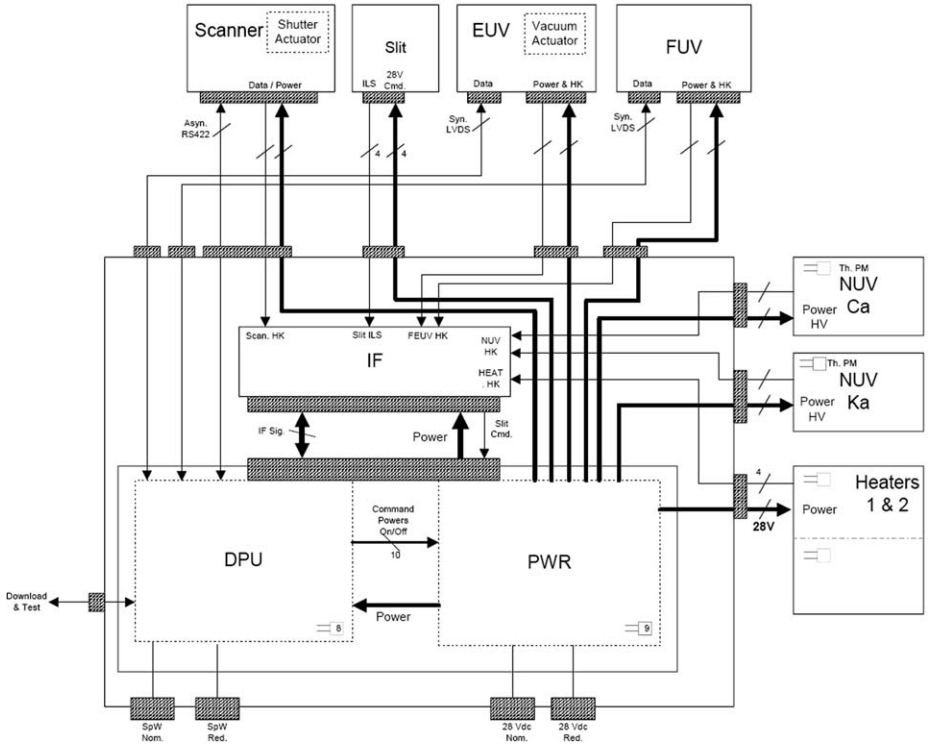

Fig. 13. PHEBUS electrical diagram.

The Power distribution unit is responsible for:

- protection/filter,
- conversion of the main bus voltage (28 V) onto all the needed secondary voltages,
- distribution of the secondary voltages to the subsystems.

4.12. Other subsystems

In order to limit the straylight inside the instrument, some internal baffles are accommodated along the optical path between the slit and the detectors. The main one is located just in front of the gratings, in order to avoid second-order pollution of one spectrometer to the other one. Another baffle is installed around the slit. A zero order trap is also installed on each detector, still with the objective to reduce the straylight level. All these baffles and traps are black coated with the same kind of absorptive treatment as used on the entrance baffle (copper oxide or equivalent), with a typical TIS factor of ~1%.

A dry nitrogen flushing system is accommodated in the vicinity of the gratings, in order to keep the inner part of PHEBUS as clean as possible with respect to dust contamination during integration activities of both instrument and spacecraft.

Due to possible outgassing of the instrument once in space, heaters are accommodated at the backside of the gratings to heat them in case of contamination.

4.13. Ressource summary

The mass of PHEBUS is 6.2 kg, its average power 3.6 W and its expected data rate 10 Mbits per orbit.

5. Science performances

5.1. Radiometric model

A radiometric model of the PHEBUS instrument, as representative as possible, has been developed (see Fig. 14). The main objectives are:

- to calculate the instrumental response, in terms of number of counts per second per Rayleigh of emission,
- to simulate observations of exospheric spectrum, and to produce detector matrix images as results,
- to anticipate real in-flight observations, in order to plan efficient observation sequences,
- to validate the scientific objectives, and to prove that PHEBUS will meet the scientific requirements,
- to provide help for technological choices, for example: EUV photocathode, slit width, number of pixels.

The radiometric model uses the current definition of the optical and technical design. It uses a combination of a ray-tracing software and numerical computing software. The ray-tracing software is used to generate optically exact images, and the numerical computing software is used to add noise effects.

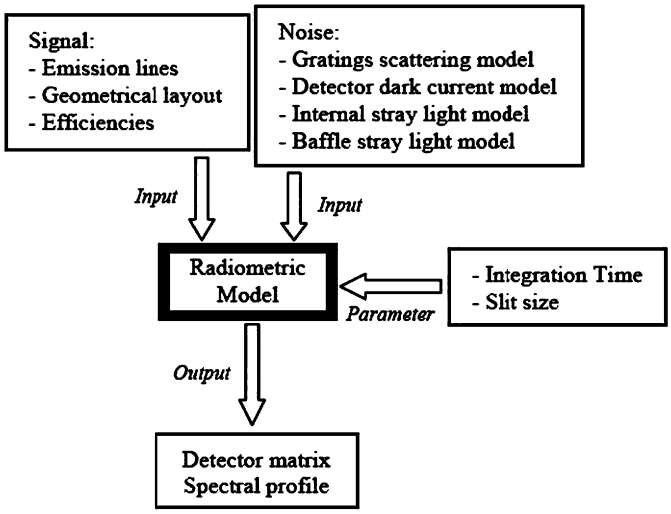

Fig. 14. PHEBUS radiometric model inputs and outputs.

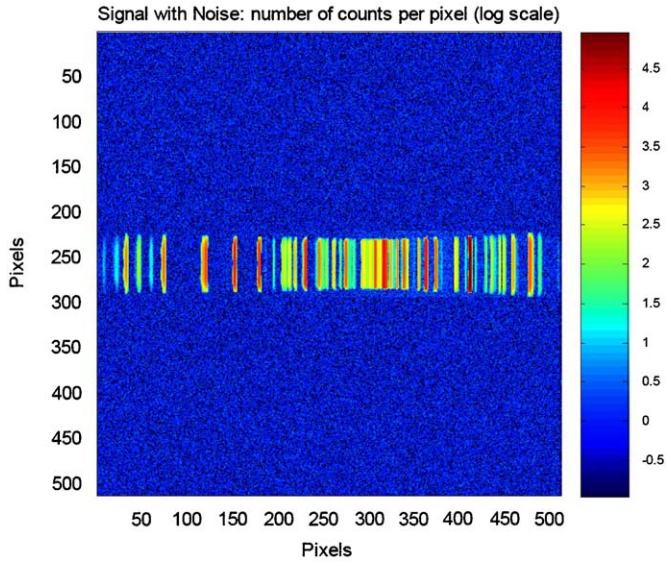

Fig. 15. Example of Detector Image Matrix (level in log-scale) with noise.

The radiometric model raw result is a matrix representing the image recorded by the detector (Fig. 15). Each pixel contains an integer number of counts, from 0 up to several thousands depending on the parameters. In order to further analyze this image, a binned spectrum profile is calculated by summing along the spatial axis of the detector (perpendicular to spectral dispersion axis) (Fig. 16).

The present model has some limits. There are large uncertainties about the expected emission lines (about a factor of 10, or more). Due to the large dynamics of detection (4–5 orders of magnitude), such possible uncertainties do not seriously affect the capacity of the instrument to measure the expected emission lines, even if

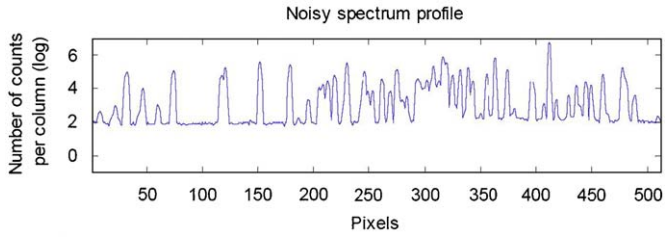

Fig. 16. Example of Binned Spectrum Profile (level in log-scale) with noise.

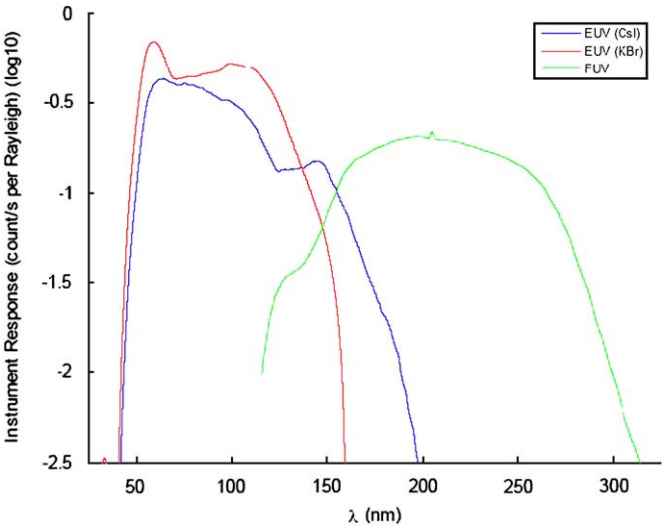

Fig. 17. PHEBUS global instrument response, for EUV (with CsI or KBr photocathode) and FUV ranges.

they are much smaller (or larger) than calculated by the model. There are also some uncertainties about efficiencies of optical components (at worst several tens of percent). The straylight and noise models are not well known in advance. Scattering by the gratings is not implemented yet. This tool will be refined with effective measurements on real optical components, and also with in-flight calibrations.

5.2. PHEBUS instrumental response

The PHEBUS instrumental response can be described as the number of counts per second per Rayleigh of emission of the source (Fig. 17). This computation is in fact the result of a combination of the instrument geometric characteristics and the components efficiencies. The mean sensitivity of PHEBUS is of the order of 0.1 count/s/Rayleigh.

5.3. Simulated spectra

With the radiometric model, examples of exospheric observations can be simulated. The positions of the emission lines are overlaid on the binned spectrum profile, in order to identify each peak of the curve. The second order of diffraction of the gratings has been also taken into account. Examples of simulated spectra are shown in Fig. 18 (EUV range) and 19 (FUV range).

The emission lines in the EUV are generally well separated. On the contrary, the FUV range is denser, with a lot of mixed emission lines.

5.4. Detectable species

There is a large dynamic range of expected emissions. Some species will be easily measured even with short integration time of less than 1 min. Other species will require accumulating observations during more than 1 h in order to become observable. Some species will remain mixed with other emission lines: for example, Xe I with S I in the EUV range, and OH with Al I in the FUV range. They can be estimated by subtraction if the other line is already known elsewhere. A mean detection limit can be estimated to about 0.1 Rayleigh for EUV, and about 0.2 Rayleigh for FUV.

A summary of the detectibility of species is given in Table 1.

6. Calibration

6.1. Ground calibration

Purpose of ground calibration procedure will be to verify the instrument performances at subsystem and system levels.

After preliminary integration and opto-mechanical alignment, ground calibration procedure of the instrument will be accomplished. Initially mechanical interfaces of the various subsystems of the instrument will be characterized according to mechanical designs and subsequent 3D measurements. In this way the relative position with respect to the optical layout design will be known within the required tolerances. Then integration with possible suitable further adjustments will be accomplished according to a detailed alignment plan. The instrument models development philosophy foresees some breadboard models which will be used to verify alignment and test procedures.

The EUV, FUV and NUV detectors will be fully characterized prior their integration on the instrument. Anode spatial resolution of EUV and FUV detector heads will be verified through modulation transfer function (MTF) measurements, performed with a periodic mask with suitable spatial frequency, and point spread function (PSF) measurements, performed with suitable projected pinhole images. Dark count rate at various high voltages and flat field response to uniform monochromatic illumination will be tested too. Some of the measurements will be performed in vacuum environment according to detector operational requirements.

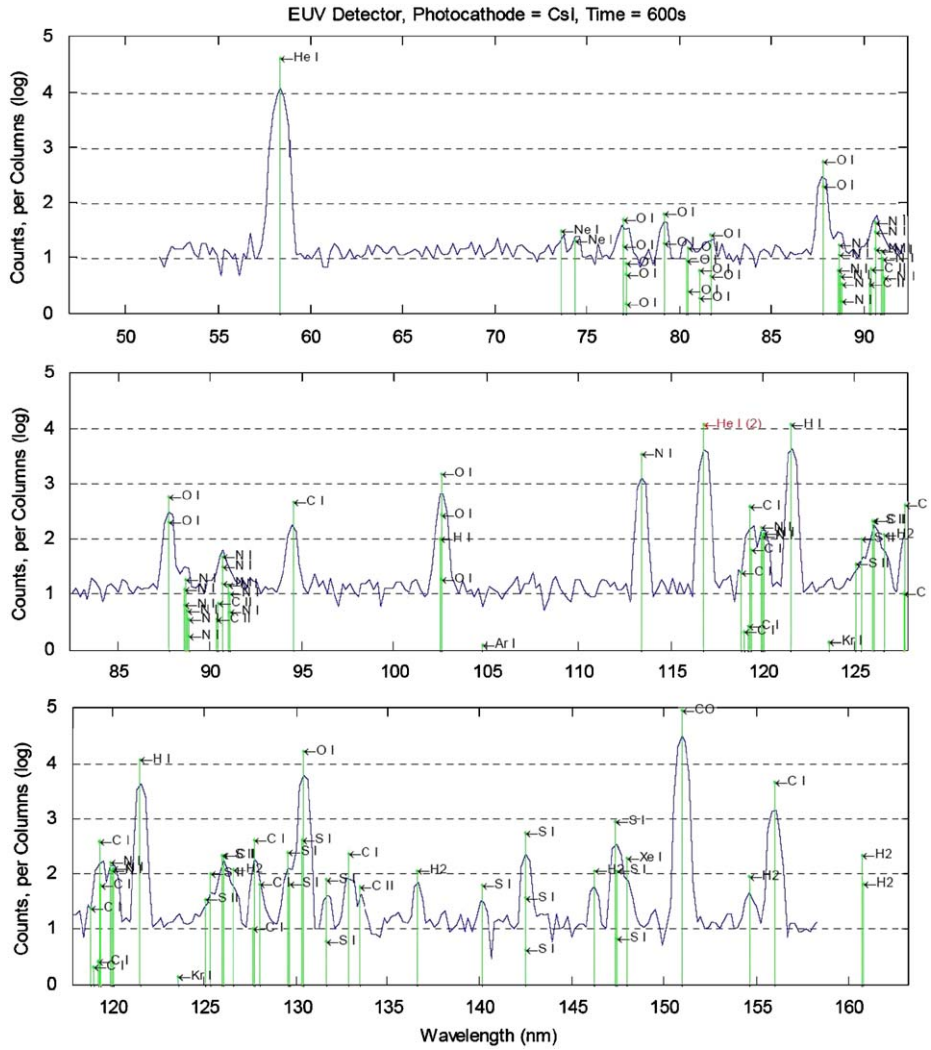

Fig. 18. EUV spectrum example, with a cumulated integration time of 10 min with nominal slit and nominal photocathode.

Diffraction gratings will be tested for their dispersion, spatial resolution and efficiency performances. For this purpose a suitable optical bench will be used, where breadboard or laboratory models of the entrance slit and detectors and gratings will be assembled. Each spectroscopic channel of the PHEBUS instrument will be finally tested after integration and alignment for verification, performance testing and radiometric calibration. These procedures will be performed with a dedicated facility consisting of a vacuum chamber equipped with EUV sources, monochromator system and projection optics. The vacuum chamber will be pumped down to residual pressure lower than 10^{-5} mbar to allow operation of open head detectors, and for cleanliness requirements residual gas analysis control will be performed. Operative vacuum conditions will be achieved with turbomolecular and cryopump systems. The chamber (about 2 m long and 0.8 m diameter) will be equipped with electrical feedthroughs and moveable mechanical supporting system to allow different relative orientation and position of the instrument. In Fig. 20 a pictorial sketch of the vacuum chamber with the instrument inside is shown: the UV beam is entering from an access window from the left. The EUV monochromatic beam will be projected with a collimating optical system in order to feed the scanning baffle-mirror system of PHEBUS; both full and partial field illumination will be considered. The instrument absolute responsivity will be derived through radiometric calibration. It will be accomplished by inserting a calibrated detector on the path of the beam entering the baffle of PHEBUS, in order to derive the relationship between detected signals and radiometric flux. The results will be finally cross-checked through the evaluation of the full instrument efficiency derived by optical design and subsystems calibration. Different UV sources will be used: a hollow cathode lamp with He–Ne gas mixture for the EUV range 55–155 nm, a deuterium lamp with MgF_2 window for the FUV range 145–315 nm, and suitable spectral sources for tests of the NUV channel. The calibration will be performed for different orientations of the instrument in

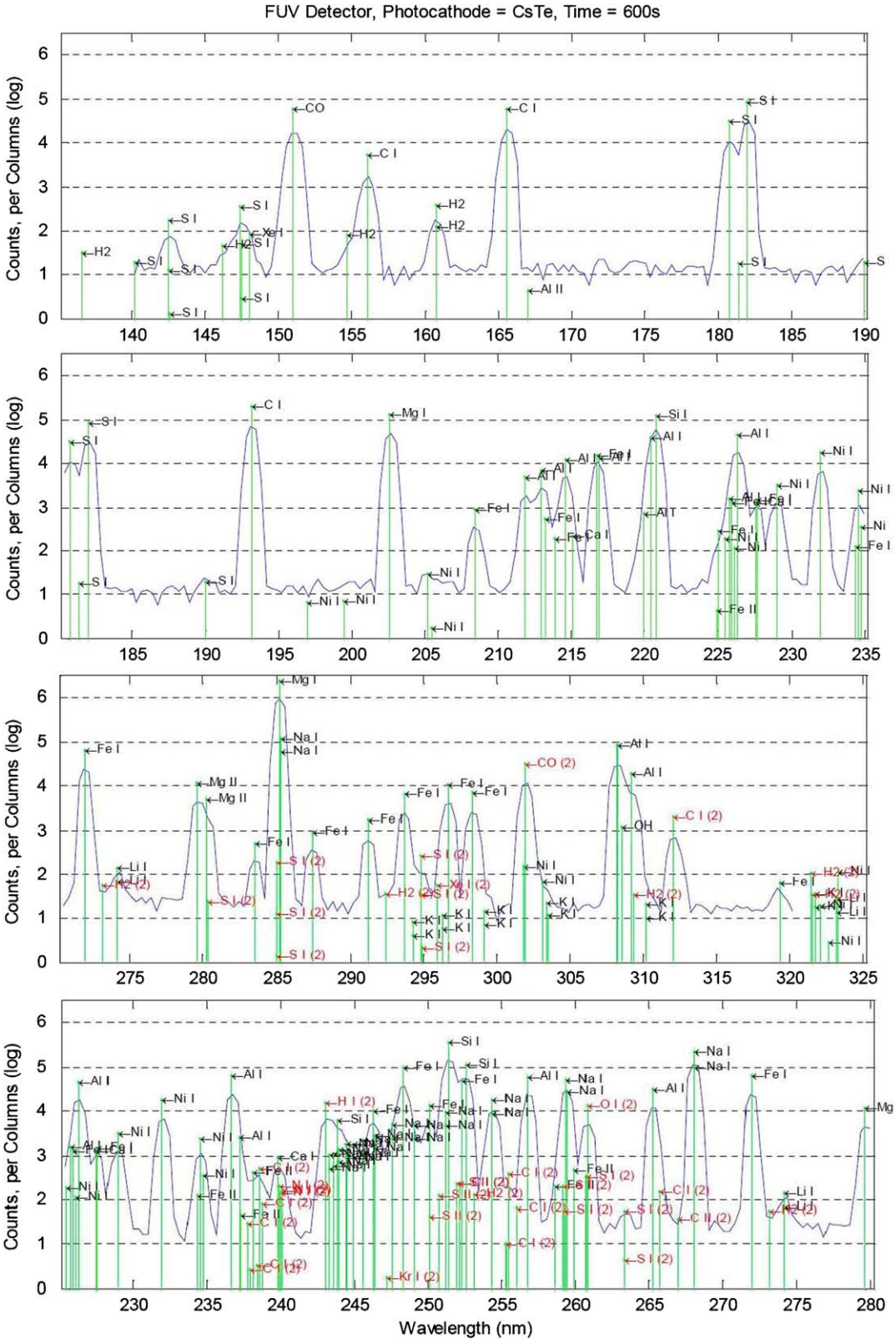

Fig. 19. FUV spectrum example, with a cumulated integration time of 10 min with nominal slit and nominal photocathode.

order to test sensitivity to polarization of radiation, to scan the whole field of view of the instrument and to evaluate the straylight rejection for sources outside the field of view. Straylight inside the instrument will be evaluated too.

6.2. *In-flight calibration*

Although ground calibrations will be necessary to acquire a good knowledge of the instrument, the length

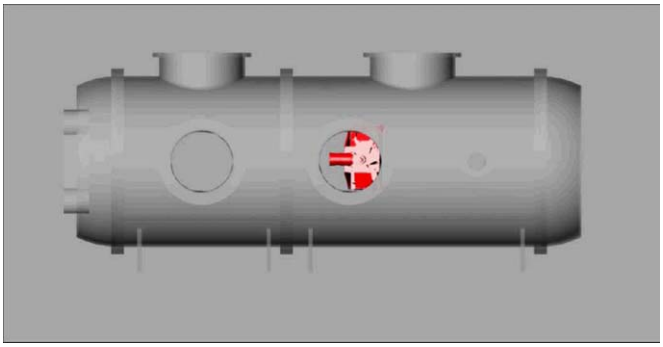

Fig. 20. Ground calibration chamber.

of the cruise to the planet and the harsh environment around Mercury will require to perform in-flight calibrations on a regular basis to follow the variations of the instrument sensitivity. Without such periodic calibrations, the knowledge of the absolute calibration would be lost rapidly and many scientific objectives would become impossible to achieve. During the cruise and around Mercury, there will be two main sources of information we can use to study the variations of the instrument calibration. First, stars can be observed on a regular basis. Many stars can be used to follow the PHEBUS FUV channel calibration. This has been made routinely by various instruments. The second source of emission is the interplanetary background caused by the resonant scattering of solar photons by hydrogen and helium atoms present in the interplanetary medium. This emission can be observed in any direction but is variable and is composed of a few lines, the helium 58.4 nm line and the H Lyman-α and Lyman-β lines.

Following Bertaux et al. (2006), we can write that the calibration factor is equal to the product of the Gain G by an efficient area S_{eff}. The efficient area, which depends on the wavelength, expresses the relation between the number of photoevents at the photocathode and the flux to be measured. For instance,

$$N(\mathrm{photoev}) = S_{\mathrm{eff}}F \quad (1)$$

where F is the incident flux in photons per surface unit per wavelength unit per time interval. N(photoev) is expressed in photons per wavelength unit per time interval. Therefore, S_{eff} is homogeneous to a surface. It expresses the efficiency of the whole instrument from the primary mirror to the photocathode and includes the grating efficiency. This quantity does not depend on the Gain of the MCP. The number of counts NC here depends on the gain of the MCP. We have the relation

$$\mathrm{NC} = GN(\mathrm{photoev}) \quad (2)$$

Therefore, since the calibration factor follows $C = \mathrm{NC}/F$, we see that it is equal to GS_{eff}. The efficient area depends on wavelength whereas the gain depends only on the MCP high voltage value and is constant with wavelength. The variation of the gain as a function of voltage can be determined easily on the ground on any source and checked at regular intervals during the mission. On the other hand, the study of the efficient area will require to look at known sources which have been observed before and are well calibrated. For the FUV range there are many available stellar sources, for instance those observed by International Ultraviolet Explorer (ESA/NASA/UK project). It is more difficult to find suitable sources for the EUV channel. A few possible sources have been identified (Wolf-Rayet stars and or Epsilon Canis Majoris).

It should be noted also that calibration on stars requires to adopt an iterative technique to avoid problems of the mixing of the different orders of scattering of the grating. This can be avoided by choosing different stars with different temperatures and propagate the calibration from longer wavelengths to shorter ones.

When the efficient area of an instrument is determined on a point source like a star, it is sometimes tricky to get the correct value for an extended source. This is often due to an uncertainty in the filling factor of the field of view, which allows to convert from a point source to an extended source. Vignetting in some parts of the field of view may also be a source of error. Finally, when estimating the efficient area from a point source, we have to make sure that the slit does not block part of the photons which would result in an overestimation of the calibration factor.

7. Observation modes

Different modes of observation will be used sequentially. These modes are defined to optimize the science return while keeping the instrument safe from degradation. The brightest sources of light are the Sun and the lit surface of Mercury. Both sources will be kept away from the LOS at all times. The baffle has been designed to achieve a 10^{-6} rejection factor at 8.2° from LOS. This means that the angular distance between the LOS and a bright source cannot be less than 8.2°. Calibrations on the actual flight model will yield a better estimate of this required safeguard angle.

During the mission, the instrument will be regularly calibrated on well chosen stars, in such a way to quantitatively estimate the overall degradation of the sensitivity of the instrument.

7.1. Exospheric science

7.1.1. Grazing sounding mode at twilight (exospheric twilight, or ET mode)

In this mode, the disk of Mercury is used as a shield against the solar light. The time of observation is chosen when the limb of Mercury is dark. The illuminated exosphere is observed near the terminator, when the spacecraft is in the night. The dark edge of Mercury can be used as a "feature", by maintaining the LOS impact parameter near 0 km altitude, in such a way to probe

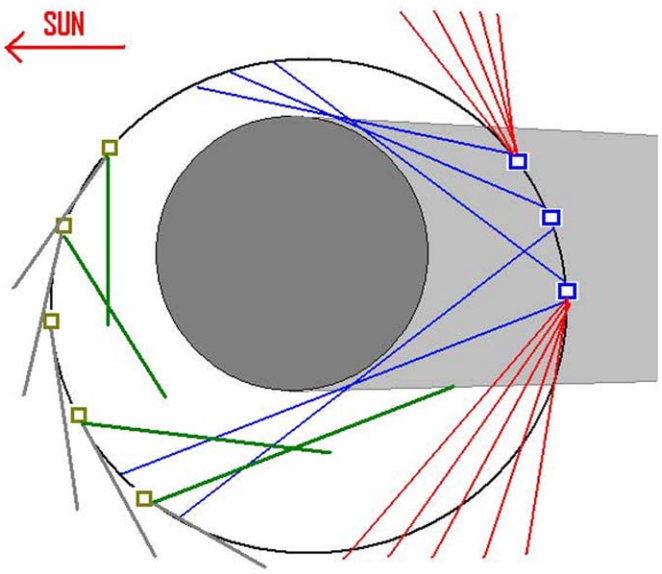

Fig. 21. Schematic view of the different observation modes. Blue lines: grazing sounding mode at twilight (ET); Red lines: vertical scanning mode (ES); Gray lines: along-orbit sounding mode with LOS parallel to the velocity vector (EO-0°); Red lines: along-orbit sounding mode with constant impact parameter (EO-200 km).

regions of altitude as low as possible, where exospheric density is high. This mode, which can be used during ingress or egress, allows a detailed observation of near-terminator regions, of particular interest in terms of exospheric dynamics and sources. It provides a natural vertical scanning of the exosphere, together with the possibility to probe very low altitudes when the tangent point is close to the terminator, allowing to search for, and measure, trace species. Active pointing is necessary, during let say 15 min before sunrise (above planetary disk), or after sunset (below planetary disk). The observation must be stopped at the time when the edge of Mercury becomes illuminated. A schematic view of this mode, and following ones, is shown in Fig. 21.

7.2. Vertical scanning mode (exospheric scanning mode)

In this mode, a vertical scan of the atmosphere, between the lowest admissible altitude (0 km if the spacecraft is in the shadow, and a yet undefined value if it is on the dayside) to, typically 1000 km altitude. The typical vertical sampling path is one half-scale height in the limb plane, that is between 20 and 100 km, depending on the targeted species, that is between 0.5° and 4° in angular unit. Because the edge of Mercury's disk is 30° below the velocity direction at periherm, and at −50° at apoherm, the baffle view axis must be able to scan the angular range from −30° to +10° at periherm, and −50° to −20° at apoherm. Typically 100 spectra will be recorded over the vertical range from the lowest possible altitude to 1000 km altitude, over a typical total time of a few tens minutes.

7.1.2. Along-orbit sounding mode (exospheric along-orbit, or EO mode)

a. If the LOS is aligned with the velocity vector of the spacecraft, looking forward (mode EO-0°), the continuous recording of the emission spectrum of the exosphere over the illuminated part of the orbit will allow to reconstruct, through differentiation, the local density of observed species along the orbit. The same can be done if the LOS is oriented in the anti-velocity direction (EO-180°).
b. Similarly, it is possible to fix the LOS at a given position, making an angle with the velocity direction. The advantage of this configuration is to reach smaller altitudes, therefore to increase the signal-to-noise ratio. Generally, the angle cannot be larger than 30° (mode EO-30°) and smaller than 150° (mode EO-150°: if so, the LOS would generally intercept the disk of Mercury at some place on the orbit, except if periherm is on the night side). Because direct illumination of the primary mirror has to be avoided, this angle has to be smaller than 30–8.2° and larger than 150+8.2°. The range of admissible angles cannot be precisely given at the present time (it also depends on the orbit, and on the position of the periherm with respect to the shadow cone of the planet).
c. Through active pointing, it is possible to maintain the LOS impact parameter at a given altitude during the whole sequence. It requires changing continuously the orientation of the LOS along the elliptical orbit, with a typical excursion of ±10° around an average angle of −40° (with respect to the velocity direction). The mode at a constant impact parameter z km is denoted by EO-z km, for example EO-100 km for an altitude of the tangent point of 100 km).

7.2. Surface mapping

7.2.1. Nightside H Ly-α reflectance mapping mode (surface Lyman-alpha mode)

In this mode, the scanning baffle view axis is pointed downward to the nadir on the night side. The reflectivity of the surface, illuminated by the interplanetary glow at 121.6 nm, is mapped in selected regions of interest, in order to search for surface ice (water, sulfur, etc.). Variations of Ly-alpha reflectivity may happen noticeably within craters of high latitude permanently in the shadow.

8. Data products

The data produced by the instrument during each observation will consist of a series of matrices extracted from the detector arrays and the two NUV detectors. These data are produced every 2 s. The data sampling is limited by the time needed to read the detector. Due to the high expected rate of parasitic counts due to energetic particles

in the harsh environment of Mercury, spectra will not be cumulated over more than the 2-s integration time in order to minimize the fraction of unusable spectra. Summation of spectra, in order to increase the signal-to-noise ratio, will be made on ground. Both EUV and FUV detector arrays are made of 256 pixels in the spatial dimension and 512 pixels in the spectral dimension. The NUV detectors are single pixel detectors. The EUV and FUV detectors will not function at the same time because of the constraint of power consumption. Therefore, every 2 s the instrument will produce, $256 \times 512 + 2$ count rate values digitized on 16 bits. This corresponds to 1 Mbit per second. If the instrument observes during 30 min each orbit, this creates a total volume of data equal to 900 Mbits per orbit which is much more than the PHEBUS telemetry budget allocation. Therefore, it will be necessary to drastically reduce the transmitted data volume. To do that, we will only transmit a fraction of the data extracted from the total array. The volume of transmitted data will be adjusted according the actual telemetry budget but will at least be equal to 3 times 512 pixel values every second which corresponds to 3 full spectra at different heights along the slit.

In most cases, we expect that the transmitted data will not be made from a single line of the array but from cumulated data, with the binning made along the spatial dimension. This will increase the signal-to-noise ratio but decrease the spatial resolution (which has no consequence since spatial resolution is provided by the scanning system). Spectral resolution can also be decreased by binning along the spectral dimension. Fig. 22 shows an illustration of such sub-arrays where cases B and C are binned over sections of the array. Case A is a full spectrum along the line of the detector array. The possibility to select which part of the detector is transmitted will allow us to optimize the science return for a given telemetry volume.

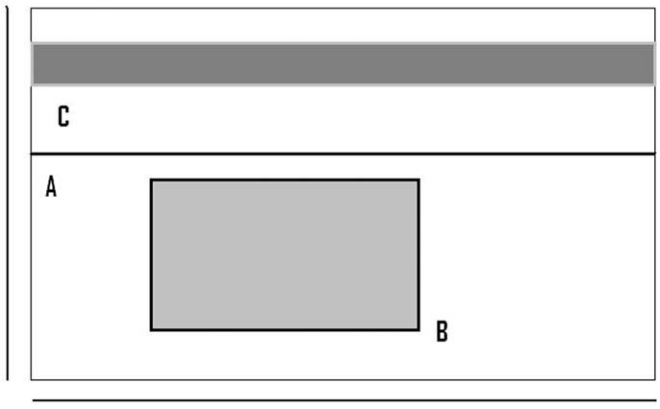

Fig. 22. Examples of binning areas on the detector array. The transmitted data will consist of lines or part of lines on the array (case A) or matrices extracted in the array (case B) or cumulation of different lines (or parts of lines) as in the case C. Binning of data could be performed in the spectral dimension (x-axis) if necessary.

9. Synergies with other instruments

9.1. Instruments on MMO

The Mercury Sodium imaging camera (MSASI) on MMO investigates the global change of sodium exosphere. This instrument can take snapshots of widely distributed sodium atoms up to a few radius of Mercury. The snapshot of Na distribution will reveal which process is responsible for production of sodium exosphere.

To investigate the structure and dynamics of the magnetized environment of Mercury, a set of comprehensive instruments is flown onboard MMO. Of particular interest for PHEBUS are the instruments dedicated to measurements of the ambient plasma, high-energy particles and energetic neutral atoms (Mercury Plasma Particle Experiment, MPPE package). The solar wind analyzer onboard MMO will allow to monitor and characterize the flow of solar ions (essentially protons) impinging the planet surface at high latitudes in the dayside sector. These measurements will place constraints on interplanetary conditions and contribute to qualify the efficiency of planetary material sputtering. Also, the mass spectrum analyzer that will be flown onboard MMO will feature a wide mass range and a high mass resolution, allowing for detailed composition measurements. Indeed it is likely that, as in the case of Earth, both solar wind and material of planetary origin contribute to the magnetospheric populations. As a matter of fact, numerical simulations suggest that planetary ions such as Na^+ may actually form a quite significant (up to a few ions cm^{-3}) plasma supply for the inner magnetosphere (e.g., Delcourt et al., 2003). After energization in the magnetosphere, these ions may be recycled via precipitation onto Mercury's surface and yield further extraction of planetary material (Leblanc et al., 2003b). Measurements from the mass spectrum analyzer will prove to be of particular interest to characterize the sources and sinks of these populations. Given the proximity of the magneto-tail current sheet inner edge with the exosphere, one also anticipates a direct response of exospheric neutrals to magnetospheric changes, which will be monitored by the energetic neutral atom (ENA) instrument onboard MMO. In particular, this instrument will allow to investigate ENA flashes (Lundin et al., 1997) that are expected to occur as a result of charge exchange during impulsive plasma injections into the near-Mercury environment.

9.2. Instruments on MPO

PHEBUS will probably not detect a large number of ion species, although some of them should be measured, depending on their abundances in the exosphere (see Table 1). The SERENA package, including the planetary ion camera (PICAM) ion imager, will provide a complementary picture of ion species, their density and velocity distribution, allowing to constrain ionized species

dynamics and exosphere-ionized species coupling processes, as well as sputtering processes at the surface. More generally, the in-situ measurements of exospheric and ionized species by SERENA will provide additional information of composition, and local densities obtained by SERENA will be used to improve retrieval algorithms applied to LOS integrated measurements made by PHEBUS. Additionally, on some orbits, PHEBUS will be pointed to the spacecraft anti-velocity direction in such a way to look at regions of the exosphere which will have been probed locally by SERENA a few minutes or 10 min before, in such a way to connect local measurements of SERENA with the more global picture provided by PHEBUS.

There is also a potentially interesting synergy with the measurements of the chemical composition of the near-subsurface material made by the MPO X-ray spectrometer (MIXS). The regolith chemical composition measured by MIXS and the fluxes of the different escaping species measured by PHEBUS, which are expected to be closely inter-related, will be compared in order to better constrain the composition of the surface and the mechanism recycling exospheric species to the regolith.

10. Conclusion

The PHEBUS instrument, due to its wide spectral range, high sensitivity and high straylight rejection rate is well suited for the study of Mercury exosphere. Understanding the way solar wind interacts with the high atmospheres of planets and the exospheres and surface of bodies with no (or tenuous) atmosphere, is a quite important goal of future planetary exploration. The combined use of UV spectroscopy and in-situ mass-energy spectrometry, as performed on BepiColombo, is a powerful means to characterize the chemical composition of exospheres, the dynamics of solar wind interaction boundaries, including planetary escape, and ultimately the fate of atmospheres and/or surfaces exposed to the long-time integrated action of solar emissions. From this point of view, the observation of the tenuous Mercury exosphere, in the most severe solar illumination and thermal conditions prevailing in the Solar System, will also constitute a test of the technique of the far and extreme ultraviolet spectroscopy as a tool to characterize Sun–planet interaction and resulting planetary evolution in the Solar System and beyond.

References

Baumgardner, J., Wilson, J., Mendillo, M., 2008. Imaging the sources and full extent of the sodium tail of the planet mercury. Geophys. Res. Lett. 35 (3), L03201.

Bertaux, J.-L., Korablev, O., Perrier, S., Quémerais, E., Montmessin, F., Leblanc, F., Lebonnois, S., Rannou, P., Lefèvre, F., Forget, F., Fedorova, A., Dimarellis, E., Reberac, A., Fonteyn, D., Chaufray, J.-Y., Guibert, S., 2006. SPICAM on Mars Express: observing modes and overview of UV spectrometer data and scientific results. J. Geophys. Res. 111, E10S90.

Bida, T.A., Killen, R.M., Morgan, T.H., 2000. Discovery of calcium in Mercury's atmosphere. Nature 404, 159–161.

Broadfoot, A.L., Kumar, S., Belton, M.J.S., McElroy, M.B., 1974. Mercury's atmosphere from Mariner 10: preliminary results. Science 185, 166–169.

Broadfoot, A.L., Shemansky, D.E., Kumar, S., 1976. Mariner 10: Mercury atmosphere. Geophys. Res. Lett. 3, 577–580.

Cremonese, G., Warell, J., Harmon, J.K., Leblanc, F., Mendillo, M., Sprague, A., 2008. Techniques and methods in ground-based observation of Mercury. Planet. Space Sci. 56, 61–78.

Delcourt, D.C., Grimald, S., Leblanc, F., Bertherlier, J.-J., Millilo, A., Mura, A., 2003. A quantitative model of planetary Na^+ contribution to Mercury's magnetosphere. Ann. Geophys. 21, 1723–1736.

Harmon, J.K., Slade, M.A., Velez, R.A., Crespo, A., Dryer, M.J., Johnson, J.M., 1994. Radar mapping of Mercury's polar anomalies. Nature 369, 213–215.

Hendrix, A.R., Hansen, J.C., 2008. Ultraviolet observations of Phoebe from the Cassini UVIS. Icarus 193, 323.

Ip, W.H., 1990. On solar radiation-driven surface transport of sodium atoms at Mercury. Astrophys. J. 356, 675–681.

Killen, R.M., Ip, W-H., 1999. The surface-bounded atmospheres of Mercury and the Moon. Rev. Geophys. 37, 361–406.

Killen, R.M., Potter, A.E., Fitzsimmons, A., Morgan, T.H., 1999. Sodium D2 Line Profiles: clues to the temperature structure of Mercury's exosphere. Planet. Space Sci. 47, 1449–1458.

Killen, R.M., Potter, A.E., Reiff, P., Sarantos, M., Jackson, B.V., Hick, P., Giles, B., 2001. Evidence for space weather at Mercury. J. Geophys. Res. 106, 20,509–20,525.

Killen, R., Cremonese, G., Lammer, H., Orsini, S., Potter, A., Sprague, A., Wurz, P., Khodachenko, M., Lichtenegger, H., Herbert, I., Milillo, A., Mura, A., 2007. Processes that promote and deplete the exosphere of Mercury. Space Sci. Rev. 132, 433.

Leblanc, F., Johnson, R.E., 2003. Mercury's sodium exosphere. Icarus 164, 261–281.

Leblanc, F., Delcourt, D., Johnson, R.E., 2003. Mercury's sodium exosphere: magnetospheric ion recycling. JGR-Planets 108 (E12), 5136.

Leblanc, F., Barbieri, C., Cremonese, G., Verani, S., Cosentino, R., Mendillo, M., Sprague, A., Hunten, D., 2006. Observations of Mercury's Na-D emission spectrum with the TNG in August 2003. Icarus 185, 395.

Leblanc, F., Chassefière, E., Johnson, R.E., Hunten, D.M., Kallio, E., Delcourt, D.C., Killen, R.M., Luhmann, J.G., Potter, A.E., Jambon, A., Cremonese, G., Mendillo, M., Yan, N., Sprague, A.L., 2007. Mercury's exosphere: origins and relations to its magnetosphere and surface. Planet. Space Sci. 55, 1069.

Leblanc, F., Doressoundiram, A., Mangano, V., Lopez-Ariste, A., Lemen, C., Gelly, B., Barbieri, C., Cremonese, G., Schneider, N., 2008. High latitude peaks in Mercury's sodium exosphere: spectral signature using THEMIS Solar Telescope. Geophys. Res. Lett., submitted for publication.

Lundin, R., Barabash, S., Brandt, P., Eliasson, L., Nairn, C.M.C., Norberg, O., Sandahl, I., 1997. Ion acceleration processes in the Hermean and terrestrial magnetospheres. Adv. Space Res. 19, 1593.

Milillo, A., Fujimoto, M., Kallio, E., Kameda, S., Leblanc, F., Narita, Y., Cremonese, G., Laakso, H., Laurenza, M., Massetti, S., McKenna-Lawlor, S., Mura, A., Nakamura, R., Omura, Y., Rothery, D., Seki, K., Storini, M., Wurz, P., Baumjohann, W., Bunce, E., Kasaba, Y., Helbert, J., Sprague, A., 2008. The BepiColombo mission: an outstanding tool for investigating the Hermean environment. Planet. Space Sci. 56, 40–60.

Potter, A.E., Morgan, T.H., 1985. Discovery of sodium in the atmosphere of Mercury. Science 229, 651–653.

Potter, A.E., Morgan, T.H., 1987. Variation of sodium on Mercury with solar radiation pressure. Icarus 71, 472–477.

Potter, A.E., Morgan, T.H., 1990. Evidence for magnetospheric effects on the sodium atmosphere of Mercury. Science 248, 835.

Potter, A.E., Morgan, T.H., Killen, R.M., 1999. Rapid changes in the sodium exosphere of Mercury. Planet. Space Sci. 47, 1441–1448.

Potter, A.E., Killen, R.M., Morgan, T.H., 2002. The sodium tail of Mercury. Meteorit. Planet. Sci. 37, 1165–1172.

Potter, A.E., Killen, R.M., Sarantos, M., 2006. Spatial distribution of sodium on Mercury. Icarus 181, 1.

Potter, A.E., Killen, R.M., Morgan, T.H., 2007. Solar radiation acceleration effects on Mercury sodium. Icarus 186, 571.

Schleicher, H., Wiedemann, G., Wöhl, H., Berkefeld, T., Soltau, D., 2004. Detection of neutral sodium above Mercury during the transit on 2003 May 7. A&A 425, 1119–1124.

Sprague, A.L., 1992. Mercury's atmospheric bright spots and potassium variations: a possible cause. J. Geophys. Res. 97, 18257.

Sprague, A.L., Kozlowski, R.W.H., Hunten, D.M., 1990. Caloris Basin: an enhanced source for potassium in Mercury's atmosphere. Science 249, 1140–1143.

Sprague, A.L., Kozlowski, R.W.H., Hunten, D.M., Schneider, N.M., Domingue, D.L., Wells, W.K., Schmitt, W., Fink, U., 1997. Distribution and abundance of sodium in Mercury's atmosphere, 1985–1988. Icarus 129, 506–527.

Sprague, A.L., Schmitt, W.J., Hill, R.E., 1998. Mercury: sodium atmospheric enhancements, radar bright spots and visible surface features. Icarus 135, 60.

Stern, S.A., 1999. The lunar atmosphere: history, status, current problems and context. Rev. Geophys. 37 (4), 453–491.

Stern, A., Gladstone, R., Retherford, K., Black, R., Scherrer, J., Slater, D., Stone, J., Feldman, P., Crider, D., 2004. The Lyman-Alpha Mapping Project (LAMP), American Geophysical Union, Fall Meeting 2004, abstract #SH54A-07.

Yan, N., Leblanc, F., Chassefière, E., 2006. Role of Caloris basin in producing short time variation of Na Mercury's exosphere. Icarus 181, 348–362.